An integrated numerical/physical approach to investigate the seismic performance of a zoned earth dam

Orazio Casablanca,* Giuseppe Di Filippo,* Luca Masini,** Fabio Rollo,** Mariagrazia Tretola***

Summary

Fully coupled time-domain dynamic numerical analyses provide a useful insight into the evaluation of the seismic performance of earth dams, taking into account factors such as partial saturation, complex soil behaviour and boundary conditions. However, the accuracy of their predictions is highly dependent on the calibration of the numerical model, either using monitoring data from real case histories or the results of small-scale models tested in the geotechnical centrifuge.

This paper describes an integrated numerical/physical approach to investigate the seismic performance of a zoned earth dam, taking into account the coupled hydro-mechanical response under both static and dynamic conditions. The numerical model was calibrated using data from a geotechnical centrifuge test on a small earth dam simulating reservoir filling and seismic loading of increasing intensity. Comparison of the results of the analyses with the data from the centrifuge test demonstrated the ability of the finite element model to reproduce the key aspects of the observed behaviour. It is shown that the integrated physical and numerical approach is effective in developing a robust and reliable prediction tool that allows the effect of the most relevant factors to be studied during extreme scenarios. Some peculiarities in the behaviour of this class of earth structures are highlighted, providing guidance for a rational assessment of their seismic performance.

Keywords: zoned earth dam, finite element analyses, centrifuge test, dynamic response

1. Introduction

As a result of global climate change, Italy, like many other countries in the world, is experiencing increasingly prolonged periods of drought, followed by short, intense rainstorms. In general, there is less rain, and the rainfall is concentrated in a very short intervals of time. The lack of rain and snow has led to a serious shortage of the country's main water resources. This has worrying consequences for the environment and the human activities that depend on it. In addition, the exceptionally intense meteorological events caused by the overheating of the earth's surface are increasing the number of landslides in an area that is already at high hydro-geological risk. In this troublesome context, dams can help to reduce these risks. They allow for the accumulation of critical water reserves, whose regulated release during dry periods mitigates the low water regime of rivers and provides irrigation water, which is vital for agriculture. In addition, the reservoirs upstream of the dams also dampen the hydraulic regimes of the rivers in the event of violent storms, mitigating floods and landslides that cause enormous economic damage to the community and, in the most severe cases, loss of life. Therefore, the scientific community's attention on the role of dams and reservoirs in the resilience of the territories most affected by climate change has increased over the last twenty years. However, in densely urbanised countries like Italy, where it is difficult to preserve the few natural areas that exist, it is even more difficult to find new suitable sites for the construction of large reservoirs. The focus should therefore be on small reservoirs, i.e. those with a storage capacity of less than 1 million cubic metres and a maximum embankment height of 15 metres, which are easier to build, and on the maintenance of existing structures, many of which are now over 50 years old on average.

On the other hand, dams also pose a significant risk in terms of seismic vulnerability, as the uncontrolled release of millions of cubic metres of water can cause extensive property damage and loss of human life. Considering that many dams are located in areas of severe seismic hazard and that most of them were built and designed in the middle of the last century without properly considering, and sometimes underestimating the seismic action, it is of utmost im-

* University of Messina, Messina, Italy
** Department of Structural and Geotechnical Engineering (DISG), Sapienza University of Rome, Rome, Italy
*** University of Sannio, Benevento, Italy

 dx.doi.org/10.19199/2024.4.0557-1405.041

portance to assess the seismic performance of earth dams to plan efficient rehabilitation measures.

Due to the transient nature of the forces involved and the complex dynamic behaviour of soils, the study of the stability of earth dams under seismic conditions has always been a challenging task for civil engineers. In the case of existing earth dams, the problem is further complicated by the lack of detailed knowledge of the recent and past loading history of the earth structure [Sica *et al.,* 2008], the soil properties and their potential changes over the service life.

The lack of reliable information on the original design of the structure, coupled with the absence of detailed monitoring, is even more relevant for small earth dams. While large dams are regularly inspected, small earth dams are often less controlled, even though the risk associated with them could be as high as for large dams.

The effects of a seismic event on an earth dam result from both the inertial forces caused by the accelerations of the earthquake and the reduction of the available shear resistance in the materials of the dam body, which is strictly dependent on the effective stress state and, consequently, on the pore pressure distribution within the embankment. In this context, the medium to coarse-grained soils used for the construction of earth dams and embankments are often partially saturated after construction and during operation [Vinale *et al.,* 1999; Mancuso *et al.,* 2003]. However, this aspect, which can significantly influence the coupled mechanical response of the soil, is commonly neglected in most of the numerical studies of the seismic response of this class of earthworks or reproduced using simplified decoupled approaches.

Numerical simulation of earth dams is usually approached in two ways. The first is to create a numerical model based on specific soil parameters and field data from an existing structure. The complexity of the constitutive model adopted may be high, provided that the field data allow the parameters to be calibrated and the state variables of the model to be initialised. To evaluate the seismic performance of the dam, target earthquakes are then applied to the model. (*e.g.,* Rampello *et al.* 2009; Sica and Pagano, 2009; Bilotta *et al.,* 2010; Elia *et al.,* 2011; Elia and Rouainia, 2013; Sica *et al.,* 2008; Charatpangoon *et al.,* 2014; Albano *et al.,* 2015; Pelecanos *et al.,* 2015; Han et *al.,* 2016; Boulanger, 2019; Sica *et al.,* 2019; Pelecanos *et al*., 2020; Biondi *et al.,* 2021; Cascone *et al.,* 2021; Sica and Dello Russo, 2021; Casablanca *et al.,* 2022, Costigliola *et al.,* 2022).

The second approach uses a simplified prototype model to highlight typical behaviour patterns (*e.g.*, Kim *et al.,* 2011; Papadimitriou *et al.,* 2014; Andrianopoulos *et al.,* 2014; Masini *et al.,* 2016, 2019, 2021; Wu *et al.,* 2021; Masini and Rampello, 2022; Irslan Khalid *et al*., 2023). Here, the constitutive laws are usually simpler, and time-domain dynamic analyses are performed to evaluate key quantities such as permanent displacements, which are intended to be indices of the seismic performance rather than predictions of dam performance.

For both mentioned approaches, fully coupled dynamic numerical analysis is now considered to be the most reliable and promising method for investigating the behaviour of complex geotechnical systems such as earth dams. They accurately simulate the geometry of the problem, the boundary conditions and the dynamic behaviour of the soil. Moreover, factors such as the complex coupled hydromechanical behaviour of soils and partial saturation of the embankment can be taken into account for a reliable pore pressure prediction [Alonso and Pinyol, 2016].

However, the calibration of the constitutive models adopted and the definition of the initial values of the state parameters still involve significant uncertainties. The availability of monitoring data from existing dams plays a crucial role in understanding the main factors influencing the seismic response of earth dams and in improving the predictive capabilities of numerical models. Unfortunately, comprehensive information on the damage mechanisms of earth dams during severe seismic events is rare, mainly due to their random nature and low probability of occurrence.

In this context, dynamic tests carried out on large (*e.g.,* Di Filippo *et al.,* 2023) and small (*e.g.,* Arulanandan and Scott, 1993; Fioravante *et al.,* 2021) scale physical models under laboratory-controlled conditions can provide a valuable insight into the system response.

There are few geotechnical centrifuge studies on dams in the literature, although their number has increased in the last twenty years. Of these, most relate to concrete dams (*e.g.,* Saleh and Madabhushi, 2010, 2011; Wang *et al.,* 2013), concrete-faced rockfill dams (*e.g.,* Kim *et al.,* 2011; Zhang *et al.,* 2019; Tian *et al*., 2023), homogeneous dams of low-permeability material and tailings dams (*e.g.,* Ge *et al.,* 2010; Izumi *et al.,* 2021; Kumar and Viswanadham, 2023; Ng *et al.,* 2023). Only a few studies refer to zoned dams with a clayey core (*e.g.,* Arulanandan *et al.,* 1993; Adalier and Sharp K., 2004; Sharp and Adalier K., 2006; Ge *et al.,* 2010; Kim *et al*. 2011; Park and Kim, 2017; Aghamolaei *et al.* 2023). One of the main reasons for the complexity of centrifuge tests on zoned dams is the operational difficulty of reproducing a small-scale model representative of the prototype, where the shell and core must be carefully constructed using materials with different physical and mechanical properties, requiring specific laying techniques.

Nevertheless, the integrated physical/numerical approach has already proven to be a highly effective strategy to study this class of earth structures and to validate the numerical model aimed at predicting their performance in different severe scenarios. Kim *et al.* [2011] conducted an integrated experimental/numeri-

cal study of the seismic response of earth-core rockfill and concrete-faced rockfill dams. Irslan Khalid *et al.* [2023] validated a finite element (F.E.) numerical model on the experimental results obtained by Kim *et al.* [2011] to develop seismic fragility curves for concrete-faced rockfill dams as a function of several seismic parameters. Recently, Ng *et al.* [2023] investigated the potential triggers and failure mechanisms of gold tailings dam failures using two centrifuge model tests and finite element back-analysis. The F.E. numerical back-analysis indicated that the instability of a tailings dam could be initially triggered in drained conditions, which could evolve into an undrained failure mechanism.

This paper presents an integrated physical/numerical approach to study the coupled hydro-mechanical response of a small zoned earth dam subjected to the seismic loadings. The study is part of the REDREEF (Risk Assessment of Earth Dams and River Embankments to Earthquakes and Floods) research project [Ventini *et al*., 2021; 2023], which aims to understand the fundamental mechanisms of the behaviour of river embankments and earth dams during potentially catastrophic events such as floods and earthquakes. A F.E. numerical model was validated based on the results of a geotechnical centrifuge test on a model zoned dam, simulating the impoundment phase and applying two seismic inputs of increasing intensity. The constitutive model adopted to describe the mechanical behaviour of the dam materials was calibrated using the results of laboratory tests performed as part of the REDREEF project to characterise the hydro-mechanical response of the materials under both fully and partially saturated conditions [Ventini *et al*., 2021; 2023].

The aim of this study is to demonstrate the validity of an integrated approach, based on centrifuge experiments on small-scale models and numerical modelling, for studying the response of very complex geotechnical systems, such as earth dams, subjected to very severe seismic events. Unlike the majority of numerical studies available in the literature, which are based on idealised schemes or case studies that often have limited geotechnical characterisation of the materials, little monitoring data during the construction of the dam and even rarer seismic records of significantly intense events, this study benefits from an integrated approach, in which: (i) the parameters describing the mechanical and hydraulic behaviour of the materials were calibrated on the basis of an extensive laboratory characterisation; (ii) the numerical model was initialised using measurements obtained from the centrifuge tests at the end of the spin-up phase; (iii) the predictive capacity of the model was assessed by comparing the computed and the observed behaviour of the earth dam subjected to seismic inputs of such intensity as to temporarily activate plastic mechanisms in the dam body; (iv) the calculation was performed using a fully coupled hydromechanical formulation; (v) the behaviour under partial saturation conditions of the materials used was explicitly modelled, albeit with a relatively simplified formulation, for the initialisation of the effective stress state in the dam body, on which the distribution of stiffness and strength depends. Finally, with reference to points (i) to (iii), it is worth noting that the numerical simulations presented hereafter can be classified as type B1 predictions according to Lambe's [1973] classification, in that the data collected during the static phases of the centrifuge tests was used to initialise the strongly non-linear response of the materials, while the dynamic response of the dam was predicted and compared with the observed behaviour.

2. Centrifuge Model Test

A dynamic centrifuge test was carried out at the ISMGEO seismic centrifuge, in Italy [Baldi *et al*., 1988; Airoldi *et al.,* 2018] to investigate the seismic response of a zoned earth dam. A scheme of the model dam is shown in figure 1.

The model was geometrically scaled down by a factor $N = 50$ and hence the design gravitational acceleration was 50 g. The dam is 260 mm high (13 m at the prototype scale), the crown and the base are 30 mm and 780 mm wide (1.5 m and 39 m), with an upstream and downstream slope of 35°, while the core base is 90 mm (4.5 m) long. The fine-grained core is made of a sandy, clayey silt named Pontida Clay (herein PON), while the flanks are made of Ticino sand (TS). After the model was accelerated up to 50 g, a viscous fluid was introduced in the upstream side to simulate the presence of a reservoir and the dam was subjected to a sequence of dynamic excitations of increasing intensity.

2.1. Tested materials

The grain size distribution curves of the tested materials are shown in figure 2, while table I summarises the index properties.

The physical and mechanical properties of the TS have been extensively studied, both in terms of static and dynamic behaviour (*e.g.,* Bellotti *et al*., 1996; Fioravante, 2000; Fioravante and Giretti, 2016; Yamashita *et al*., 2000), while the hydro-mechanical properties and the mechanical behaviour of Pontida clay have been recently investigated by Ventini *et al*. [2021; 2023] and by Ventini and Mancuso [2024].

2.2. Model preparation and instrumentation

This section reports a synthetic description of the centrifuge test and of the instrumentation setup, while more detailed information on the experimental activity can be found in a companion paper [Casablanca *et al.,* 2024]. The model was constructed in a rigid

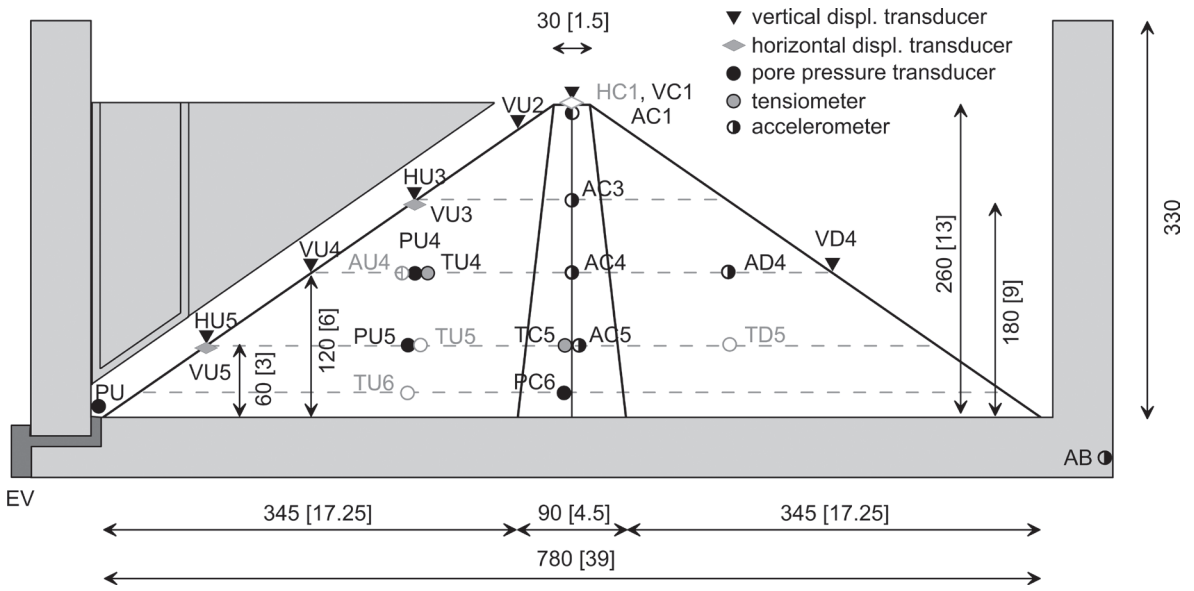

Fig. 1 – Geometry of the centrifuge model and instrumentation. Dimensions are given in mm on the centrifuge model scale and in m on the prototype scale (in brackets).

Fig. 1 – Schema del modello in centrifuga e della strumentazione installata. Le dimensioni sono indicate in mm alla scala del modello in centrifuga e in m alla scala del prototipo (tra parentesi).

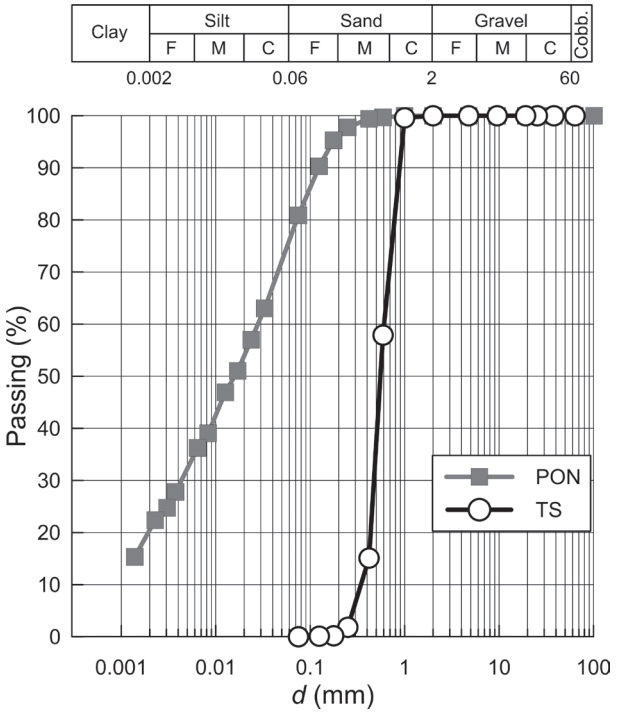

Fig. 2 – Grain size distribution of the testing soils.

Fig. 2 – Distribuzione granulometrica dei terreni impiegati nella prova in centrifuga.

box with internal dimensions of 800 mm in width × 395 mm in depth × 330 mm in height (Fig.1), intending to model plane-strain conditions. The silty core was compacted to the Optimum Proctor Standard water content and dry density, as detailed in table II.

Compaction was carried out in strata of 2 cm of thickness and 9 cm of width, up to the final height, then the core was trimmed to the final trapezoidal shape. Once the core was shaped, the box was progressively filled with sand compacted at a relative density of 80% (Tab. II) and finally the flanks of the dam were shaped by progressively trimming the sand to the final shape. During the reconstitution process, the monitoring transducers were located at the designed position displayed in figure 1. The dam body was extensively instrumented with miniaturized tensiometers, T, pore pressure transducers (PPT), P, accelerometers, A, located upstream (U), downstream (D) and in the core (C). An additional accelerometer was fixed to the base of the model container to measure the time history applied by the shaking table (AB). Linear displacement transducers and roto-translative sensors allowed to monitor vertical (V) and horizontal (H) displacements. In figure 1 empty symbols with grey lettering indicate malfunctioning instruments. The tensiometers can measure both positive

Tab. I – Index properties of the testing soils.

Tab. I – Proprietà indice dei terreni impiegati nella prova in centrifuga.

Soil	γ_{min} (kN/m^3)	γ_{max} (kN/m^3)	e_{min}	e_{max}	G_s	D_{50} (mm)	FC (%)	IP (%)
Ticino (TS)	13.64	16.67	0.574	0.923	2.68	0.53	0	-
Pontida Clay (PON)	-	-	-	-	2.77	0.017	81	11

Tab. II – Reconstitution details.
Tab. II – Caratteristiche del modello in centrifuga.

Dam zone	N. strata	Strata thickness (m)	w (%)	γ_d (kN/m^3)	γ (kN/m^3)	D_R (%)	e (-)
Core (PON)	13	0.02	16	17.72	20.45	-	0.534
Sides (TS)	13	0.02	5	15.74	16.53	80	0.669

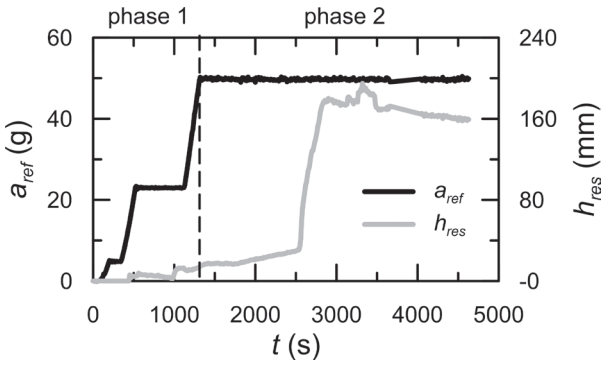

Fig. 3 – Time histories of the gravitational acceleration and reservoir level at the model scale.
Fig. 3 – Storie temporali dell'accelerazione in centrifuga e del livello dell'invaso alla scala del modello.

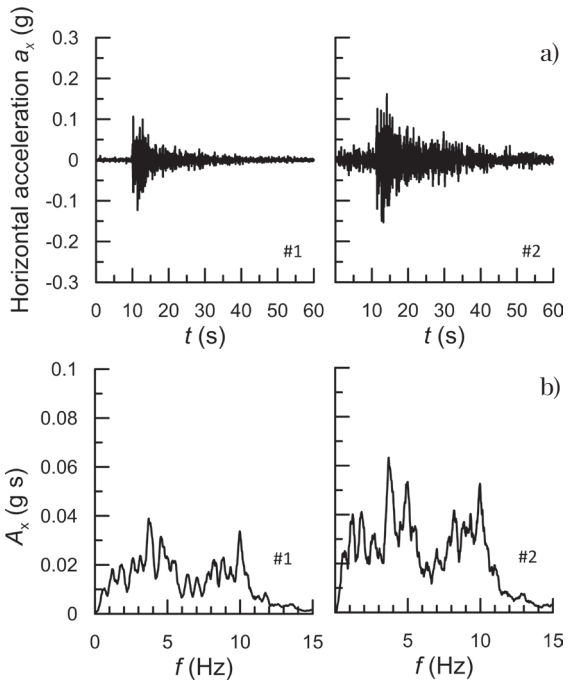

Fig. 4 – Input motions applied during the test: a) time-histories; b) Fourier spectra.
Fig. 4 – Input sismici: a) storie temporali; b) spettri di Fourier.

and negative pore pressures (*i.e.,* suctions), while the PPTs only read positive values. Further detail on the specifics of the sensors can be found in Casablanca *et al.* [2024].

The fluid used to model the reservoir was stored in an external tank connected to the model via a controllable pipe fitted with an electric valve, and a pressure transducer (PU, Fig. 1) monitored the reservoir level. A viscous fluid with a viscosity 50 times greater than that of water, called hydroxypropylmethylcellulose (HPMC), was used to match the scaling ratios for time in diffusion and dynamic phenomena [Kutter, 1995; Taylor, 2018]. In addition, a profiled steel wedge based on the shape of the dam flank was used to limit the volume of fluid required to simulate the presence of the reservoir and to limit the inertial effects of the reservoir during the simulation phases. The wedge is made of two steel profiles rigidly connected to the box and separated by a cavity for housing the measuring instrumentation.

As illustrated in figure 3, the impoundment system was pre-tested by briefly opening the inlet valve at 20 g. This caused a limited rise in the reservoir level. The impoundment was then completed when the centrifuge reached the target acceleration (50 g) in a single stage of about 3000 s at the model scale (4h 10min at the prototype scale).

A final level of 160 mm was reached, which is equivalent to a reservoir level of 8 m at the scale of the prototype. The arm of the centrifuge was also equipped with a single-degree-of-freedom shaking table, which allowed to apply two subsequent acceleration time histories characterised by similar transient waveforms but increasing intensity, as shown in figure 4 in terms of time-histories and Fourier spectra.

The seismic parameters for the two input motions used in the test are detailed in table III and are characterised by the same predominant frequency (f_P) but different values of the Arias intensity (I_a).

3. F.E. Simulation

The numerical analyses of the earth dam were performed at the prototype scale in plane strain conditions through the Finite Element code PLAXIS 2D [Bentley, 2021]. The domain is discretised in 4523 triangular 15-node elements, with a total of 37035 nodes (Fig. 5). The 15-node elements are characterised by 4th order interpolation for displacements and 3rd order for strains, which allows to obtain a satisfactory accuracy in case of coupled u-p analyses. Soil behaviour is modelled through the Hardening Soil

Tab. III – Seismic parameters of the input motions.
Tab. III – Caratteristiche degli input sismici.

Test	ID	PGA (g)	I_a (m/s)	f_P (Hz)	B-width (Hz)
2	#1	0.123	0.134	3.70	3.58-10.08
	#2	0.162	0.418	3.69	3.55-10.05

model with Small Strain Stiffness (*HSsmall*) [SCHANZ *et al.*, 1999; BENZ *et al.*, 2009].

Partial saturation is taken into account through two state variables, obtained from the combination of the total stress σ and the pore water pressure u_w and the air pore pressure u_a. In detail, Bishop's effective stresses [BISHOP and BLIGHT, 1963] are employed according to the expression:

$$\sigma=\sigma'+\chi u_w+(1-\chi)u_a \quad (1)$$

where σ' is the effective stress and χ is the matrix suction coefficient varying from 0 to 1 and depending on the degree of saturation, porosity and the matric suction (u_a-u_w). In PLAXIS formulation, the pore air pressure u_a is neglected, while the coefficient χ is assumed to be equal to the effective saturation $S_r^{eff}=(S_r-S_r^{res})/(S_r^{sat}-S_r^{res})$, where S_r^{sat} is the degree of saturation for saturated soils and S_r^{res} is the residual degree of saturation (*i.e.,* the part of fluid that remains within pores even for high suctions). In light of above, equation (1) becomes:

$$\sigma=\sigma'-S_r^{eff}\cdot(u_a-u_w) \quad (2)$$

where the term $S_r^{eff}\cdot(u_a-u_w)$ is defined as effective suction.

It is worth noting that in this study the partial saturation does not affect the soils constitutive response, unlike more advanced models in the literature (*e.g.* ALONSO *et al.,* 1990; BUSCARNERA and NOVA, 2009; ZHOU *et al.,* 2015; ROTISCIANI *et al.,* 2021). Also, the hysteresis of the retention curves upon wetting-drying paths is neglected.

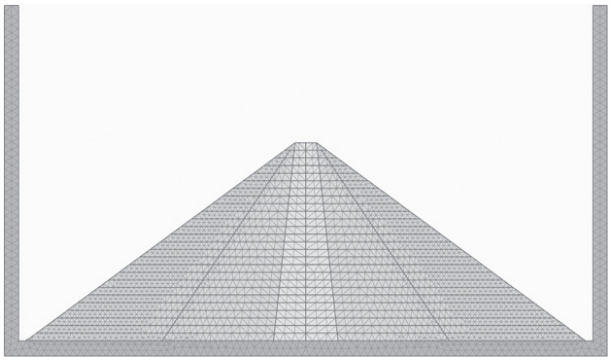

Fig. 5 – Numerical model of the dam and element discretisation.
Fig. 5 – Reticolo di calcolo agli elementi finiti.

Despite the relatively simple formulation used for partial saturation, Bishop's stress approach represents an acceptable compromise as it allows the distribution of stiffness and mobilised strength to be accurately reproduced before and during the seismic events.

To properly analyse the time-dependent mechanical behaviour of saturated or partially saturated soils, it is essential to consider both deformation and groundwater flow by adopting the coupled hydromechanical approach, which requires simultaneous solutions to the mixed equations of displacement and pore pressure. This approach incorporates the well-established Biot's consolidation theory to describe the interaction between the solid and pore fluid phases. In this formulation, two equations are solved simultaneously to determine displacements (u) and pore pressures (p), commonly known as the u-p formulation [ZIENKIEWICZ and SHIOMI, 1984]. These equations govern the momentum equilibrium of the soil-water mixture and the mass balance for the pore water, and an implicit Euler integration method is used to solve these governing equations efficiently [GALAVI, 2010]. According to ZIENKIEWICZ *et al.* [1980], the u-p formulation provides a more accurate solution to dynamic problems than the simplified undrained approach for permeability values greater than 10^{-4} m/s, typical of medium clean sands. For the range of material permeabilities and input motion frequencies adopted in this study, the u-p formulation provides reliable results with relatively little computational effort compared to more advanced formulations (*e.g.* ARGANI and GAJO, 2022). Therefore, the u-p formulation is adopted here to simultaneously calculate deformation and groundwater flow in the body of the dam with time-dependent boundary conditions and in presence of seismic actions.

The numerical analyses were carried out according to the following phases, in accordance with the centrifuge test model: (1) initialisation of the model stress state through the instantaneous activation of the model weight; (2) initialisation of the suction field, assuming a simplified linear distribution approximating the pore pressures measured at the beginning of the test; (3) impoundment phase, progressing in two stages until the water level reaches 8 metres; (4) dynamic phase, involving the application of the two input movements at the base of the model.

The F.E. model explicitly included the box containing the dam model. Preliminary elastic dynamic analyses were carried out to determine the equivalent stiffness to be applied under plane strain conditions. The aim was to match the first fundamental frequency of the 2D model box to that of the real 3D box. The box was modelled as a non-porous material. To simulate the seismic inputs applied by the centrifuge shaking table, the same time histories of horizontal displacements were applied to the bottom boundary of the model, ignoring any potential radiation attenua-

tion sources in the F.E. model, while the vertical degree of freedom was fixed. The vertical boundaries of the box were left unrestricted to replicate experimental conditions.

3.1. Model calibration

The *HSsmall* model is an isotropic hardening elasto-plastic model, in which the elastic region is bounded by two yield surfaces, a shear hardening yield surface and a cap yield surface, whose evolutions are controlled by deviatoric and volumetric plastic strains, respectively. The former can expand up to the Mohr-Coulomb failure criterion and is characterised by a non-associated flow rule, while an associated flow rule is employed for the latter. Within the elastic domain, the formulation is hysteretic para-elastic according to the Masing's rules and incorporates a modified version of the Hardin and Drnevich [1972] hyperbolic law to reproduce the shear modulus reduction curve and soil damping from small to medium and large strain levels. The small strain shear stiffness G_0, as well as the secant stiffness E_{50}, the unloading-reloading modulus E_{ur} and the oedometric modulus E_{oed} depend on the current stress state by means of a function of the minor principal effective stress and the strength parameters c' and φ'.

In the numerical model, saturated unit weight γ_{sat} of 20 kN/m^3 and 19.2 kN/m^3 are assigned to Ticino sand and Pontida clay, respectively. The parameters of the *HSsmall* model, summarised in table IV, have been calibrated against the results of a series of laboratory tests carried out in both static and dynamic conditions as a part of the PRIN REDREEF research project.

Results of drained triaxial compression tests were used to select the strength parameters and soil stiffness at medium and large strain levels. In the case of Pontida clay, isotropically consolidated drained triaxial compression tests were performed for different values of initial mean effective pressure p' [Ventini and Mancuso, 2024], while for the Ticino sand, results of isotropically and anisotropically consolidated drained triaxial compression tests were carried out on samples characterised by relative density from 72.5 % to 90 %.

Figure 6 shows a comparison between the stress-strain curves in terms of deviatoric stress q and axial strain ε_a obtained from experiments and from numerical simulations, while figure 7 shows the failure envelops in the p'-q plane. As both materials exhibit softening behaviour, two failure conditions corresponding to the peak and post-peak strength have been identified: for the latter, the pairs (p', q) corresponding to the axial strain ε_a equal to 20 % and 10 % for PON and TS, respectively, have been chosen to reproduce the stress-strain response in a strain interval representative of the problem under study. The adoption of the post-peak strength parameters c' and φ' in the numerical analyses is motivated by the limitation of the *HSsmall* model to reproduce brittle behaviour, as highlighted in figure 6.

Tab. IV – *HSsmall* model parameters used in the numerical analyses.

Tab. IV – Parametri del modello costitutivo HSsmall assunti nelle analisi numeriche.

Parameter	Ticino sand	Pontida clay
c' (kPa)	1.0	14
φ' (°)	41	34
ψ (°)	0	0
E^{ref} (MPa)	396	228
E/E_{50}	20	26.8
E_{50}/E_{oed}	1.40	1.55
E_{50}^{ref} (MPa)	19.8	8.5
E_{oed}^{ref} (MPa)	14.1	5.5
E_{ur} (MPa)	59.4	27.1
ν_{ur}	0.2	0.2
G_0^{ref} (MPa)	165	95
$\gamma_{0.7}$	1.7e-4	1.7e-4
m	0.50	0.98
R_f	0.85	0.80

For the Ticino sand, only the isotropically consolidated specimens t32, z16 and z6, characterised by relative densities of 72.5 %, 78.8 % and 83.7 %, are shown in figure 5b for the sake of brevity. The failure ratio R_f, denoting the ratio between the failure deviatoric stress and the asymptotic value of q, is assumed equal to 0.85 for TS and 0.8 for PON. The secant modulus E_{50}^{ref} has been calibrated to reproduce the stiffness at the large strain levels of the q-ε_a curves in figure 6. In the absence of specific experimental data, the oedometric modulus E_{oed}^{ref} has been assumed to be a fraction of E_{50} (1.40 and 1.55 for Ticino sand and Pontida clay, respectively) and the unloading-reloading modulus has been assumed to be $E_{ur} = 3E_{50}$.

The dynamic response of Ticino sand was investigated by the ISMGEO research group in the context of the *PRIN REDREEF* research project, while Pontida clay by Fioravante and Jamiolkowski [2005]. As shown in figure 2, Pontida clay (PON) is a sandy and clayey silt, characterised by 57 % of silt, 23 % of sand and 20 % of clay. Consequently, the experimental results for Ticino sand (TS) and Pontida clay (PON) are similar in terms of normalised shear modulus. The parameter $\gamma_{0.7}$ was selected to fit the experimental shear modulus reduction curves shown in figure 8a, while the damping curve (Fig. 8b) is an outcome of the *HSsmall* model. The shear modulus G_0^{ref} at the reference pressure p_{ref} = 100 kPa and the constant m were evaluated to reproduce the stress dependency proposed by Bellotti *et al.* [1996] and Fioravante and Jamiolkowski [2005], leading to the shear stiffness profile with depth reported in figure 8c. Finally, the earth

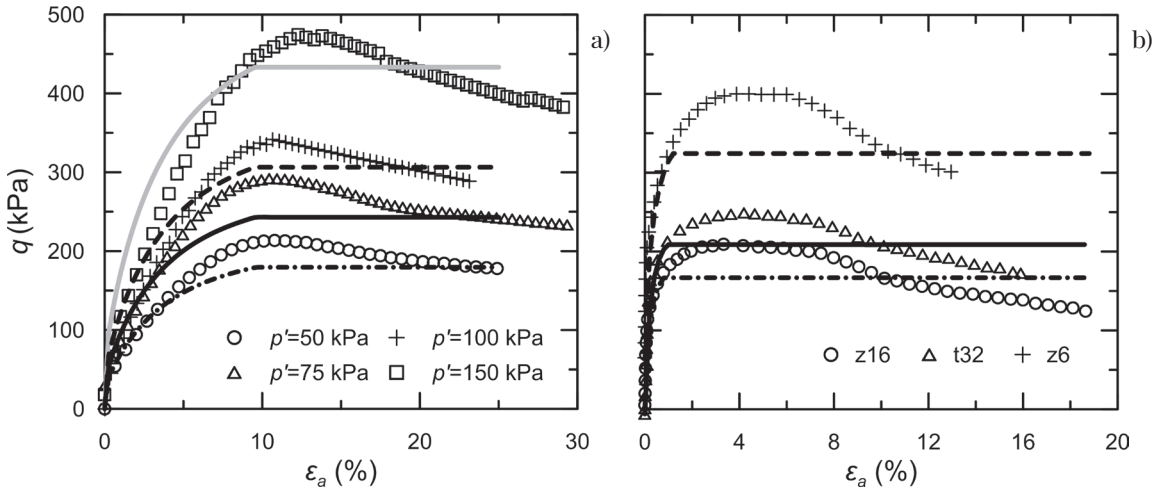

Fig. 6 – Stress-strain curves from isotropically consolidated drained triaxial compression tests on a) Pontida clay samples, b) Ticino sand samples (z16: p' = 45 kPa, *e* = 0.648; z6: p' = 100 kPa, *e* = 0.631; t32: p' = 56 kPa, *e* = 0.67).

Fig. 6 – Curve tensione-deformazione ottenute da prove di compressione triassiale drenate consolidate isotropicamente su a) campioni di argilla di Pontida, b) campioni di sabbia del Ticino (z16: p′ = 45 kPa, e = 0.648; z6: p′ = 100 kPa, e = 0.631; t32: p′ = 56 kPa, e = 0.67).

pressure at rest coefficient is determined through the Jaky's formula $K_0^{nc} = 1 - \sin\varphi'$ [Jaky, 1944].

Despite the inability to reproduce strain-softening behaviour, the *HSsmall* model represents a reasonable compromise between accuracy and complexity of the simulation, since it allows to take into account the nonlinear stress-strain behaviour of the soil, with the occurrence of irreversible strains from the beginning of a loading process, the dependence of the stiffness on the effective stress state and on the past loading history, the significant change in stiffness during unloading and the hysteretic behaviour during cyclic loading.

The constitutive assumptions have been deliberately chosen to keep the complexity of the analyses at a level comparable to that characterising modern best practice in dam engineering, in order to demonstrate the ability of a well-known constitutive model to reproduce the main factors influencing the seismic behaviour of earth dams, provided that the model is calibrated using the results of a careful geotechnical characterisation. This pragmatic choice was driven by the intention to provide research results that could be directly applied in engineering practice. Obviously, the above approach leads to less advanced, though possibly more reproducible, results compared to pre-

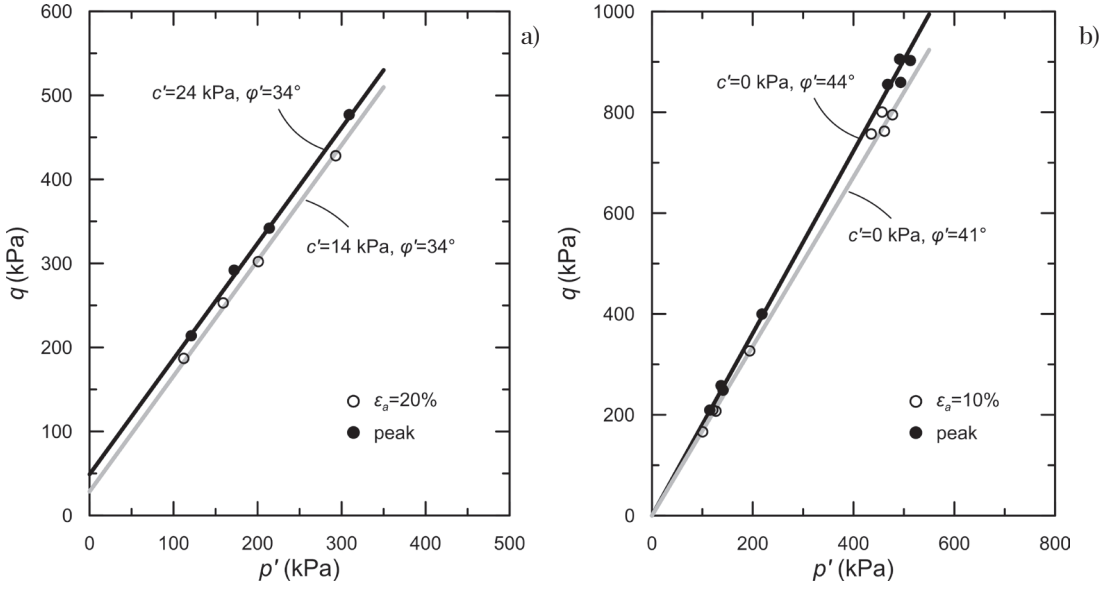

Fig. 7 – Failure envelops for a) Pontida clay and b) Ticino sand.

Fig. 7 – Inviluppi di rottura per a) argilla di Pontida e b) sabbia del Ticino.

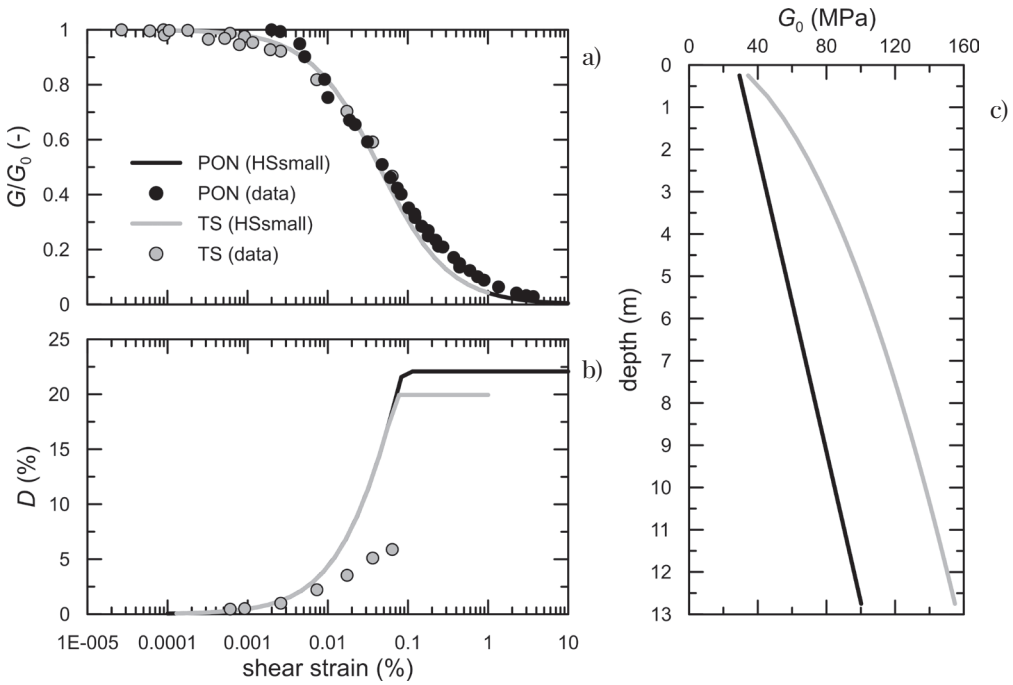

Fig. 8 – Dynamic properties of the tested soils: a) shear modulus reduction curves; b) damping curves; c) profiles of the small strain shear stiffness with depth.

Fig. 8 – Proprietà dinamiche dei terreni: a) curve di decadimento del modulo di taglio; b) curve di smorzamento; c) profili della rigidezza a taglio iniziale con la profondità.

dictions made using more sophisticated constitutive models, which, however, are hampered by the difficulty of initialising the often large number of state parameters in complex geotechnical systems such as earth dams.

The hydraulic properties of the tested soils have been part of the experimental activity carried out within the PRIN REDREEF research project. In detail, measurements of the saturated hydraulic conductivity and the hydro-mechanical response of Pontida clay compacted using both distilled water and HPMC were comprehensively studied by Ventini and Mancuso [2024]. The results of the research show that the use of HPMC significantly affects the soil-liquid retention curve of the fine-grained PON and its hydraulic behaviour in both saturated and unsaturated regimes, while no effects are detected for the TS due to its high saturated permeability. To account for the effects of partial saturation of the soils in the centrifuge tests, Van Genuchten's model [Van Genuchten, 1980] has been adopted in the numerical analyses. According to this, the current degree of saturation depends on the suction level through the expression:

$$S_r(\psi) = S_r^{res} + (S_r^{sat} - S_r^{res})\left[1+(g_a|\psi|)^{g_n}\right]^{g_c} \quad (3)$$

Where ψ is the pressure head and g_a, g_n and g_c are model parameters. Accordingly, the soil permeability depends on the effective degree of saturation via the equation:

$$k_{rel}(S_r) = \max\left\{S_r^{eff\,g_l}\left[1-\left(1-S_r^{eff\,\frac{g_n}{g_n-1}}\right)^{\frac{g_n-1}{g_n}}\right]^2, 10^{-4}\right\} \quad (4)$$

where k_{rel} denotes the relative permeability (*i.e.* the ratio between the current permeability and that of the fully-saturated soil) and g_l is a model parameter. Figure 9 shows the comparison between the retention curves predicted by the Van Genuchten model and the available experimental data, and table V reports the model parameters adopted in the analyses.

Typical values have been adopted for the parameter g_l as no direct experimental results are available. Finally, in order to better reproduce the time-de-

Tab. V – Hydraulic properties and parameters of the Van Genuchten model.

Tab. V – Proprietà idrauliche e parametri del modello di Van Genuchten.

Parameter	Ticino sand	Pontida clay
k_{sat} (m/s)	1.72e-3	2.83e-10
S_{res}	0.156	0.330
S_{sat}	1	1
g_n	5.00	1.16
g_a (m^{-1})	6.38	0.45
g_c	-0.800	-0.137
g_l	0.50	-4.63

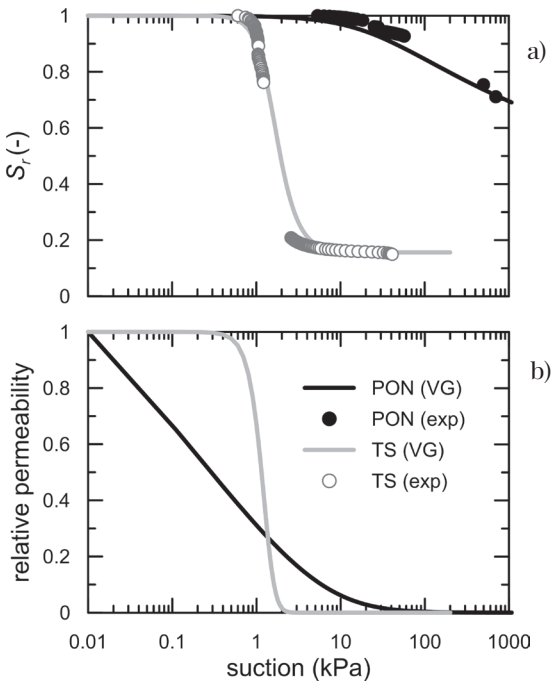

Fig. 9 – Retention curves of the tested soils (exp) and prediction of Van Genuchten's model (VG): a) degree of saturation and b) relative permeability.

Fig. 9 – Curve di ritenzione (exp) e previsione del modello di Van Genuchten (VG): a) grado di saturazione e b) permeabilità relativa.

pendent hydraulic behaviour and the distribution of the pore pressures observed during the centrifuge test, it was necessary to assume a higher saturated permeability for the TS (k_{sat} = 1.73×10^{-3} m/s) than that measured under laboratory conditions (k_{sat} = 3.3×10^{-5} m/s).

Prior to the dynamic calculation, it is essential to accurately reproduce the distribution of mobilised stiffness and shear strength in the dam, both of which are affected by the effective suction field developed during the static phases. In this respect, the construction of the model induced an almost constant suction of about 26 kPa in the upstream slope. A similar value was initially recorded by TC5 in the core. Therefore, the FE model was initialised by imposing a uniform suction distribution in the upstream slope (dashed lines in Fig. 11), while in the core, due to the different construction procedure [CASABLANCA *et al.,* 2024], a hydrostatic distribution was applied based on the only available suction measurement (TC5).

3.2. Comparison between predicted and observed behaviour

A comparison between the observed and computed dam behaviour is presented in the next sections in terms of pore pressures, displacements and accelerations. A distinction is made between the static and the dynamic phases. Herein, the data are reported at the prototype scale, unless otherwise stated. Negative pore pressures indicate suction, vertical displacements are assumed to be positive if upward, horizontal displacements are assumed to be positive if directed downstream. The same sign convention is used for accelerations.

In the following, data from instruments with technical problems (marked in grey in Fig. 1) are not included in the discussion of the results.

3.2.1. STATIC PHASE

After initialisation of the pore pressure distribution in the absence of the reservoir, a fully coupled calculation phase was performed to simulate the impoundment phase. Specifically, a time-dependent hydraulic head condition was applied to the upstream face of the dam to reproduce the experimental reservoir filling history plotted in figure 3. Figure 10a shows the pressure measured at the bottom of the reservoir by ppt PU during the impoundment phase and the time history assumed at the same location as a result of the time-dependent boundary condition applied to the upstream slope.

Figure 10b and figure 10c plot the measured and computed pore pressure in the upstream shell during the impoundment phase. A close match was obtained for the ppt PU5 and the tensiometer TU5, which were placed at the intermediate level. The trend of the pore pressure calculated at the highest level (transducers PU4 and TU4) is in qualitative agreement with the experimental data. However, it should be noted that the final value measured by both the PU4 and TU4 transducers (around 35 kPa) does not seem to correspond to the level of the reservoir at the end of the impoundment phase.

The pore pressure measured in the core by the ppt PC6 and the TC5 tensiometer (Fig. 10d and Fig.10e) is correctly reproduced by the F.E. model. The response of the two transducers in the fine-grained core was significantly slower than that of the instruments in the coarse-grained flanks, due to the very low permeability of the core (about 10^{-10} m/s) and showed an increasing tendency at the end of the impoundment phase. It can therefore be inferred that the seismic inputs were applied before the model had reached steady-state hydraulic conditions.

This observation is supported by the comparison of the pore pressure contours obtained from the FE analysis at steady state (Fig. 11a) and after the impoundment phase (Fig. 11b), corresponding to a reservoir level of 8 m. No differences are observed in the coarse-grained shells, indicating the immediate achievement of steady-state conditions. Conversely, the pore pressure in the fine-grained core at the end of the impoundment is significantly different from the long-term steady-state conditions.

Figure 11c shows the contours of the effective degree of saturation (S_r^{eff}). As the TS is characterised by a very steep water retention curve (Fig. 9a), a small in-

crease in suction beyond the air entry value causes a rapid desaturation of the material to the residual degree of saturation (S_r^{res}). As a consequence, after the impoundment phase, it is $S_r^{eff} = 0$. in the downstream flank and in the part of the upstream flank located above the free surface ($u = 0$), where the effective suction (not shown for the sake of brevity) is therefore zero ($\chi = 0$). Conversely, the desaturation of the PON is much slower as the suction increases (Fig. 9a), leading to values of S_r^{res} of up to 75 % in the upper part of the core. It can therefore be concluded that partial saturation largely affects the fine-grained core of the dam, resulting in a much higher effective stress state than would have been obtained by neglecting partial saturation. On the other hand, the effective stress state in the flank is not affected by partial saturation. It should be noted that this result should not be generalised as it depends on the water retention curve of the materials.

Figure 12 shows the calculated pore pressure profiles before and after the impoundment phase. The vertical alignment of the sensors upstream (U) and in the core (C) is shown in figure 12a, while the horizontal alignment 5 is shown in figure 12b. Data measured during the centrifuge test are also shown in the same figure. The measured pore pressure was averaged from the two transducers where both tensiometer and PPT readings were available at the same location. As the PPTs are not capable of measuring suction, when the tensiometers measured negative values (suction), only the readings from these instruments were considered. No data are available for the downstream shell.

The relatively rapid impoundment of the reservoir induced positive pore pressures in the coarse-grained upstream flank. The wetting front only reached the lower part of the core, while a slight decrease in suction was observed in the upper part, with a value of 14 kPa at the end of impoundment. The same response was obtained from the fully coupled analysis (full lines in Fig. 12), which shows a satisfactory agreement with the experimental data, although some pore pressure fluctuations are observed in the core (Fig. 11b and Fig. 12b) possibly due to the difficulty of the calculation algorithm in handling the governing equations with the very large permeability contrast between the TS and the PON .

Figure 13 shows the measured and computed geometry of the embankment obtained at the end of the impoundment phase. The arrows and cross symbols indicate the start and end positions of the reference points. Table VI reports the displacements measured at the end of the impoundment phase and the values obtained from the analyses at the same location of the transducers.

The displacements observed at the end of the static phase are negligible, except for the VU4 transducer (44 cm, 3.3%H), which probably underwent a local movement when it came into contact with the viscous fluid during the flooding phase. The results of the numerical analyses agree well with the observed behaviour, although with values even lower than those obtained experimentally (Tab.VI). The patterns shown in figure 13 (magnification factor = 3) indicate that the dam has not suffered any signif-

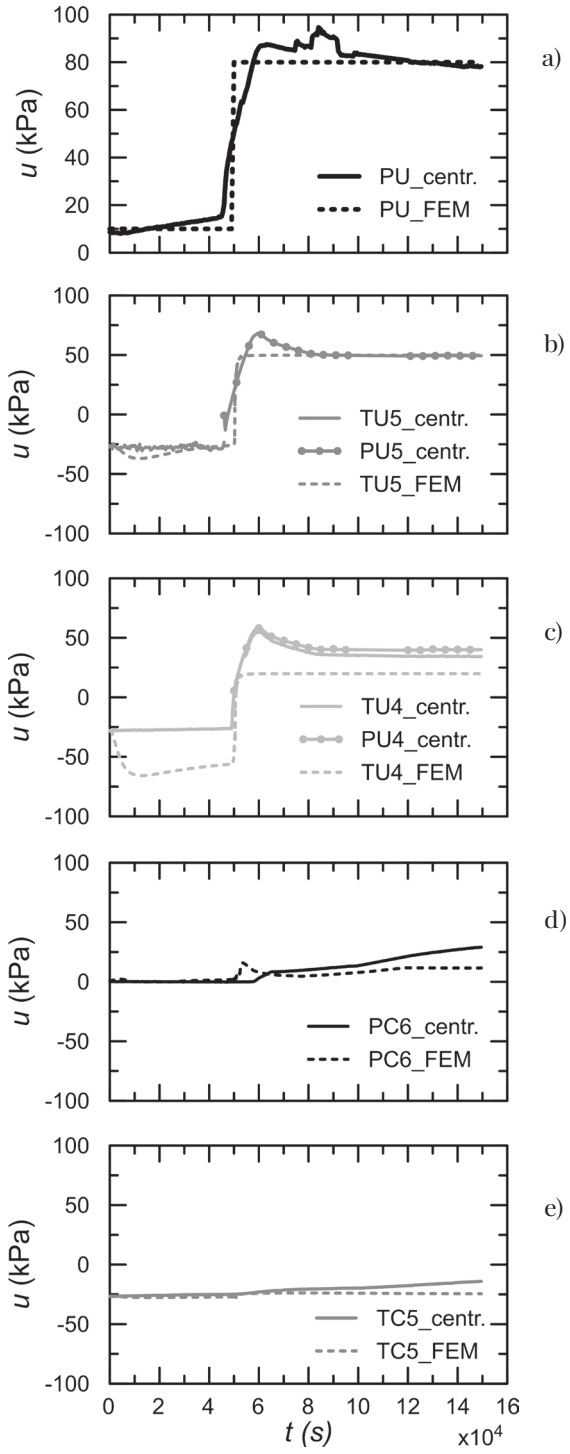

Fig. 10 – Computed and measured time histories of the pore pressures during the impoundment phase: a) in the reservoir; b) and c) in the upstream shell; d) and e) in the core.

Fig. 10 – Storie temporali della pressione interstiziale calcolata e misurata durante la fase di invaso della diga: a) alla base dell'invaso; b) e c) nel fianco di monte; d) ed e) nel nucleo.

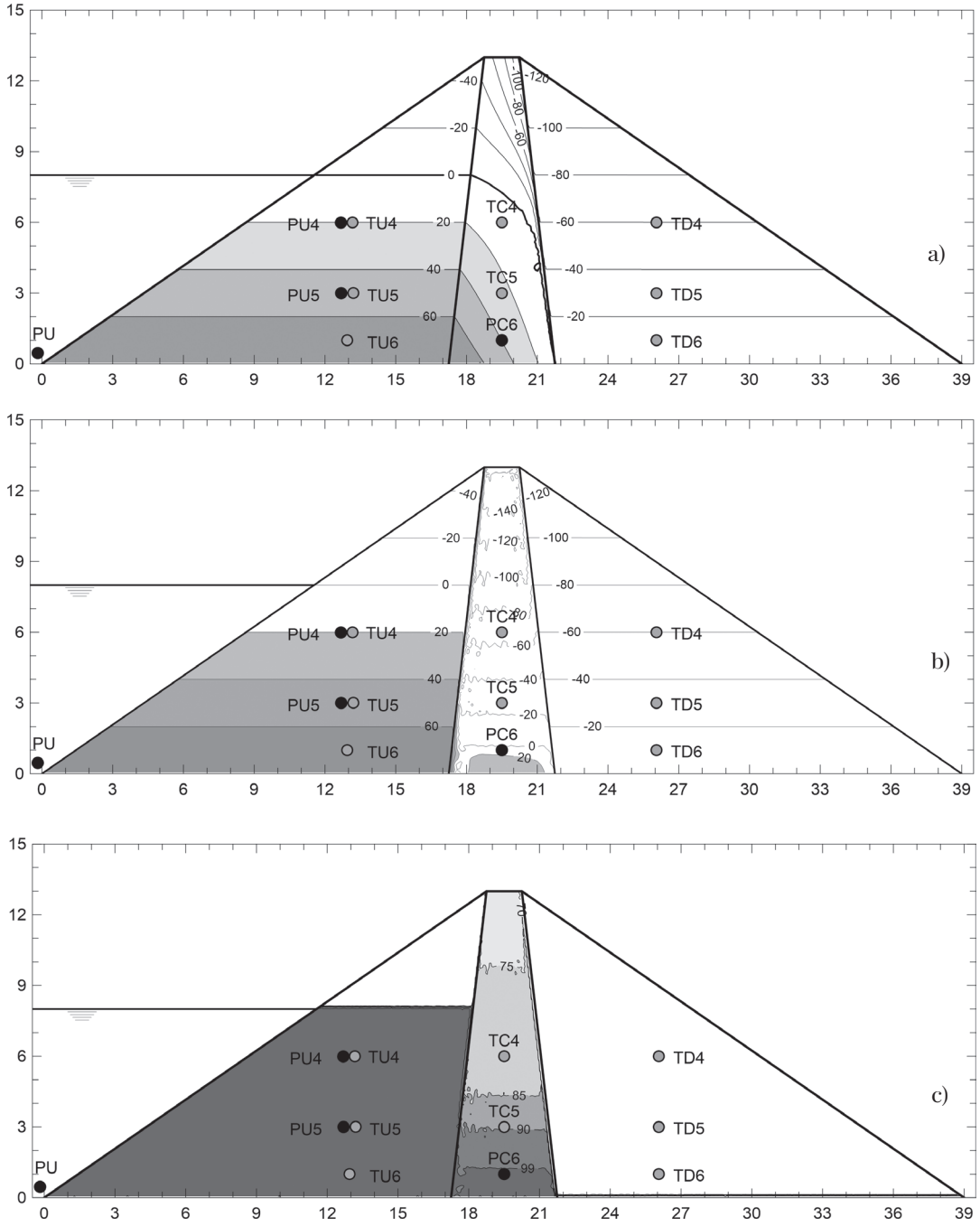

Fig. 11 – Contour of the computed pore pressure: a) steady-state conditions; b) at the end of the impoundment phase (values in kPa); (c) contour of the effective degree of saturation (S_r^{res}).

Fig. 11 – Isolinee della pressione interstiziale calcolata: a) in condizioni stazionarie; b) alla fine della fase di invaso (valori in kPa); (c) isolinee del grado di saturazione efficace al termine dell'invaso (S_r^{res}).

icant deformation or damage from the impoundment of the reservoir. It should be noted that the numerical analysis predicts some uplift of the portion of the upstream slope located below and slightly above the final reservoir level (up to 0.01%H at VU3), which can be attributed to the reduction in effective stresses as the wet front propagates into the upstream shell. Conversely, some settlement (close to 0.01%H at VU2) is predicted in the upper part of the upstream flank and in the core. However, the magnitude of these displacements is negligible for engineering purposes.

3.2.2. Dynamic phase

Figure 14a shows the measured and computed horizontal acceleration-time histories a_x at the crest of the dam, along with the corresponding Fourier am-

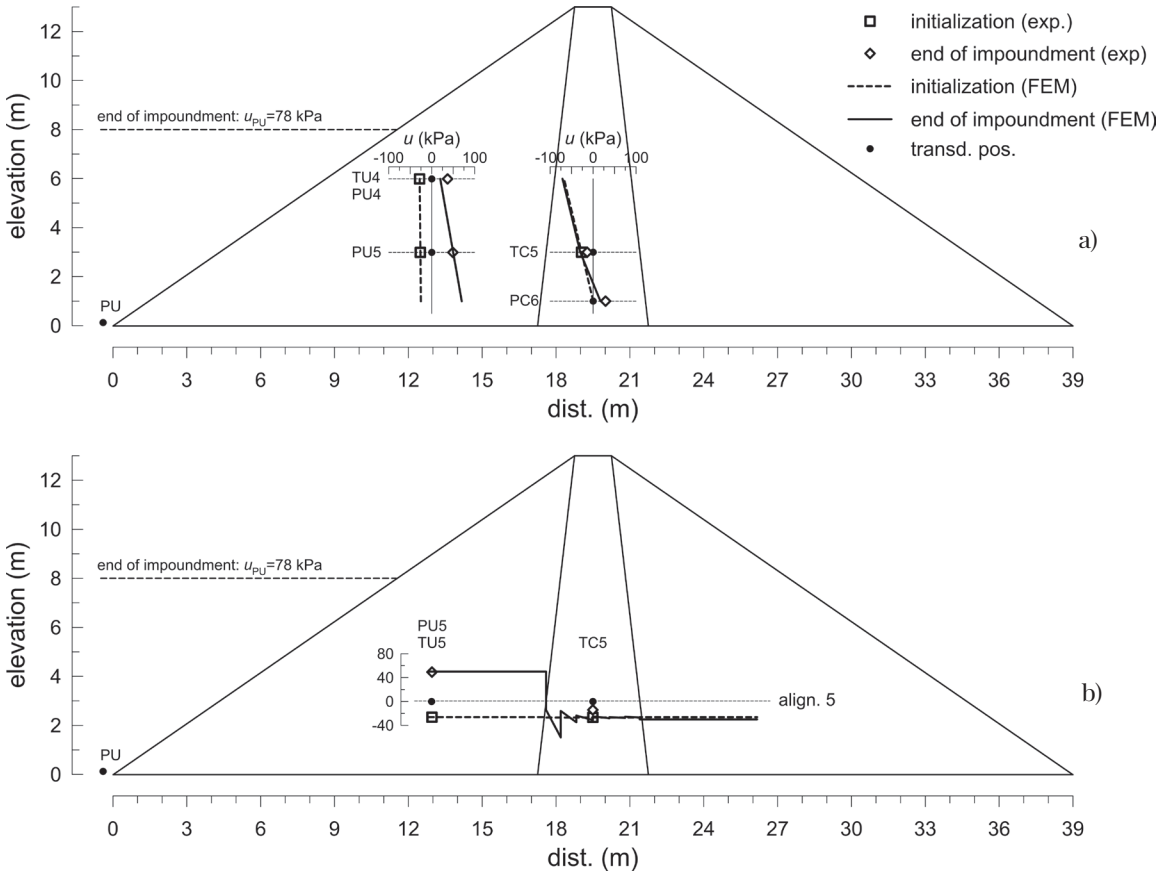

Fig. 12 – Profiles of the pore pressures before and after the impoundment: a) along the two vertical alignments of sensors, upstream (U) and in the core (C), b) along the horizontal alignment 5.

Fig. 12 – Profili della pressione interstiziale prima e dopo l'invaso: a) lungo i due allineamenti verticali dei sensori installati nel fianco di monte (U) e nel nucleo (C), e b) lungo l'allineamento orizzontale 5.

plitude spectra A_X (Fig. 14b), and the amplification function (Fig. 14c).

During the centrifuge test, the acceleration was monitored through accelerometers PCB (grey line) and MEMS (dark grey line). Both experimental and numerical results show that the crest acceleration experiences considerable amplification, although the maximum acceleration values measured by the PCB and MEMS are rather different. The maximum crest acceleration recorded by the PCB is 0.54 g for input #1 and 0.94 g for input #2, while the corresponding values obtained by the MEMS are 0.35 g and 0.5 g, re-

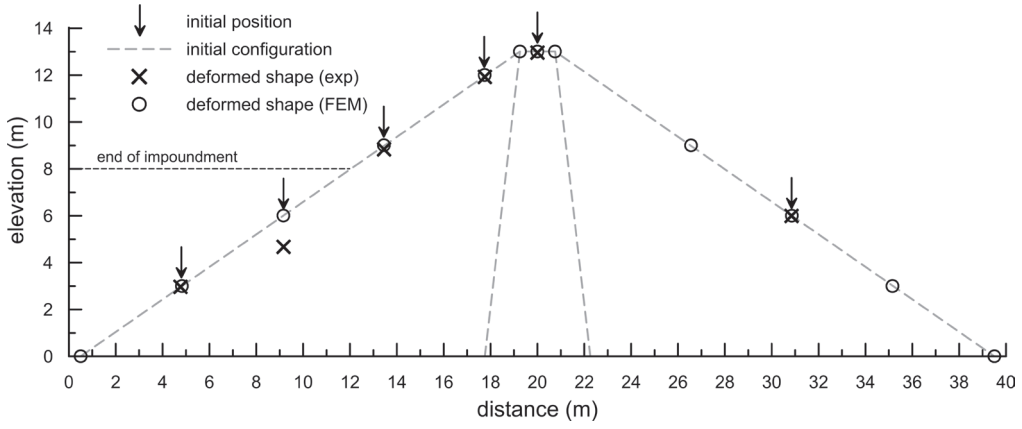

Fig. 13 – Deformed shape of the dam at the end of the impoundment: experiments vs numerical results (magnification factor = 3).

Fig. 13 – Confronto tra la configurazione deformata della diga misurata e calcolata al termine dell'invaso (fattore di ingrandimento = 3).

Tab. VI – Displacements (values in cm) at the end of the static phase: experimental vs numerical results.
Tab. VI – Spostamenti misurati e calcolati al termine della fase statica (valori in cm).

Transducer	centrifuge	FEM
VC1 (ver.)	-1.65	-0.088
HC1 (hor.)	1.92	-0.125
VU2 (ver.)	-2.84	-0.144
VU3 (ver.)	-5.84	0.155
HU3 (hor.)	-0.02	-0.206
VU4 (ver.)	-44.4	0.075
VU5 (ver.)	-1.29	0.033
HU5 (hor.)	-0.21	-0.011
VD4 (ver.)	-0.41	-0.002

spectively. This difference is possibly ascribed to the different sensitivities of the two transducers [CASABLANCA *et al.*, 2024]. The maximum crest acceleration predicted by the F.E. analyses is 0.39 g for input #1 and 0.49 g for input #2, suggesting a better agreement with the values measured by the MEMS.

The Fourier spectra of the two signals monitored at the top show a similar frequency content between 3.6 Hz and 5.6 Hz, with the predominant frequencies around 4.0 Hz and 4.9 Hz for inputs #1 and #2, respectively. The F.E. simulations are consistent with the observed behaviour in that the computed Fourier spectra are characterised by a predominant frequency of approximately 5 Hz and a frequency content between 4.5 Hz and 5.5 Hz. The peak of the amplification functions shown in figure 14c occurs at frequencies of 4.5 Hz and 5.5 Hz for inputs #1 and #2,

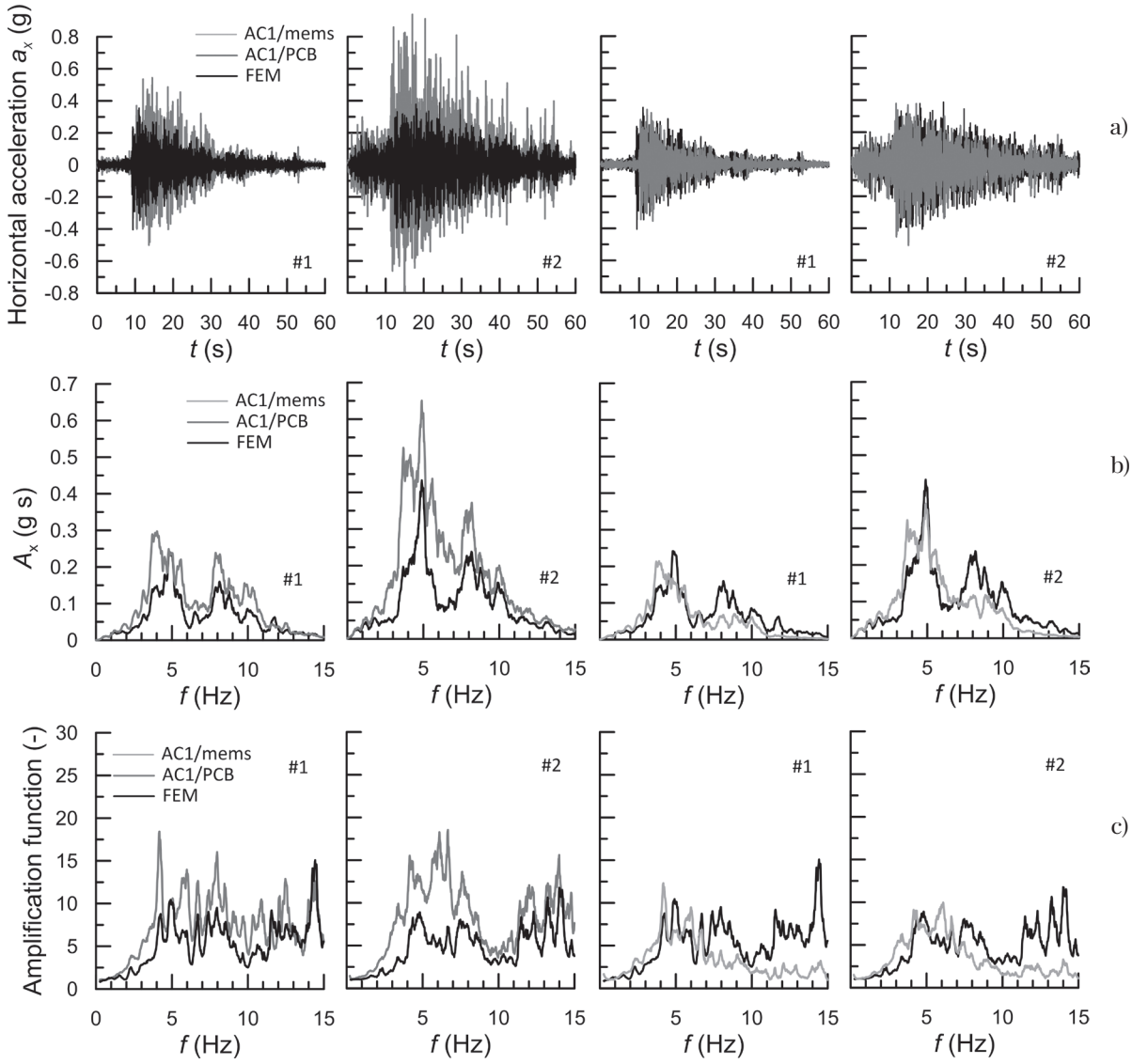

Fig. 14 – Measured and computed horizontal acceleration at the crest of the dam: a) time-histories; b) Fourier spectra; c) amplification function.
Fig. 14 – Accelerazione orizzontale misurata e calcolata al coronamento della diga: a) storie temporali; b) spettri di Fourier; c) funzione di amplificazione.

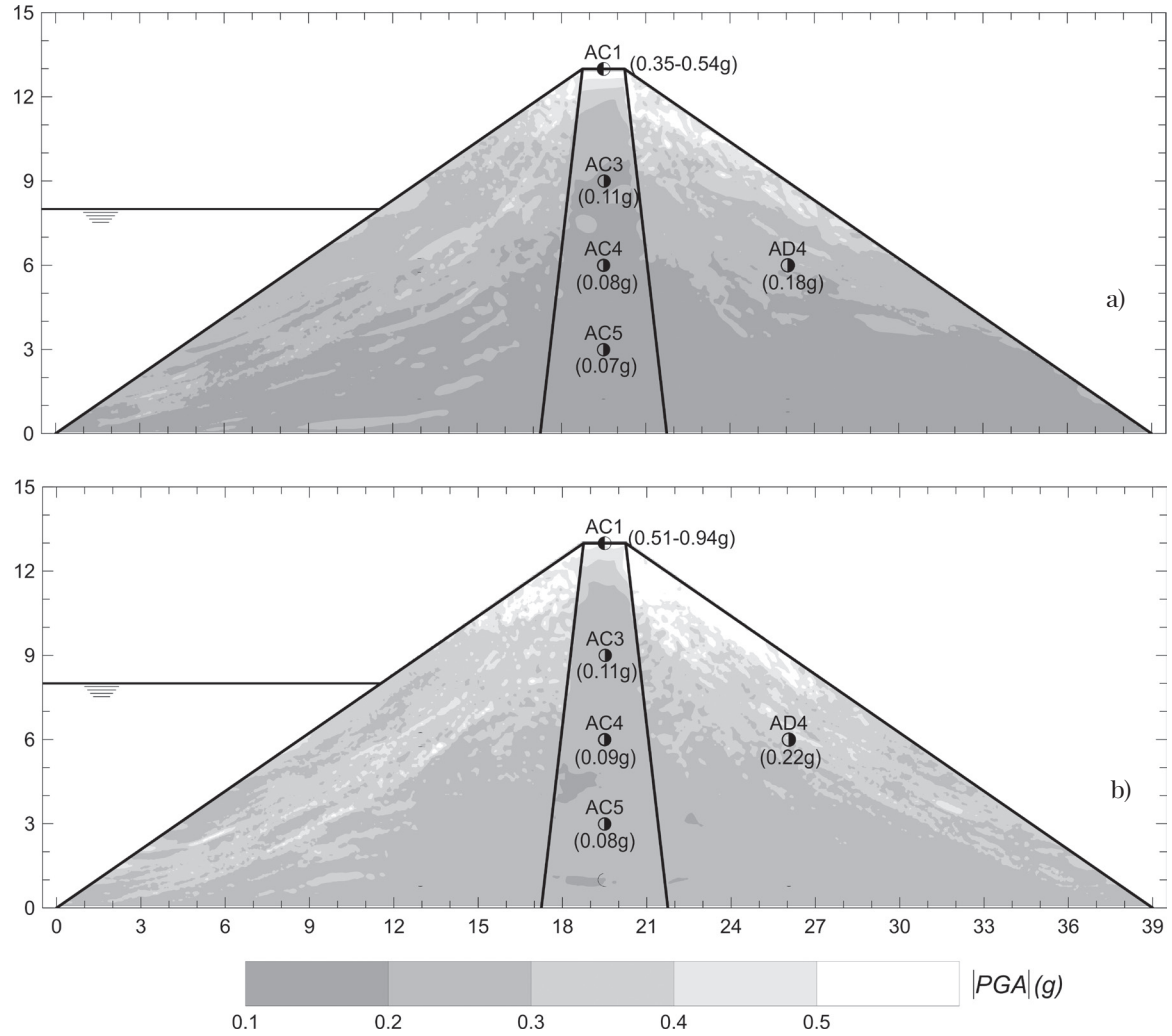

Fig. 15 – Contours of the computed absolute maximum acceleration (PGA) for a) input #1 and b) input #2.
Fig. 15 – Isolinee dell'accelerazione massima assoluta calcolata (PGA) per l'input a) #1 e b) #2.

respectively. Therefore, the estimated natural frequency of the dam in the centrifuge test is about 5 Hz, very close to that obtained numerically. This appears to be hardly affected by the amplitude of the applied acceleration, suggesting a quasi-linear response of the fine-grained core. This result is supported by the large amplification factors at the crest, with values between 20 and 30, and the small displacements measured by the transducers at the top of the dam. Therefore, it can be inferred that the shear strength of the fine-grained core of the dam was not attained during the seismic shaking.

Figure 15 shows the contour maps of the maximum absolute acceleration (*PGA*) computed for input #1 (Fig. 15a) and #2 (Fig. 15b); the values of *PGA* measured in the centrifuge are also given in the same figure. The maximum values of *PGA* predicted by the FE model are located close to the crest of the dam as a result of the focalisation of the shear waves propagating in the dam. The *PGA* is always lower than 0.5 g for input #1, while it reaches values of about 0.6 g for input #2, especially in the upper part of the downstream flank.

Figure 16 shows the profile of the maximum accelerations in the core and in the downstream flank, normalised to the maximum acceleration of the input (PGA/PGA_{inp}). In the figure, data from PCB (full circle) and MEMS (empty circle) are distinguished, while FEM results are represented by lines. The normalised acceleration increases with height. The maximum recorded PGA/PGA_{inp} values are 2.9 (MEMs) and 4.4 (PCB) for seismic input #1, and 3.1 (MEMs) and 5.8 (PCB) for seismic input #2. The PGA/PGA_{inp} profile obtained from the F.E. analyses is representative, on average, of the values measured in the centrifuge, while a closer agreement between the FEM results and the experimental data is observed in the downstream flank for both seismic inputs.

Figure 17 plots the time histories of the excess pore pressures (Δu) during the sequence of the two seismic inputs in the upstream shell and in the core. Here, Δu is defined as the difference between the current value

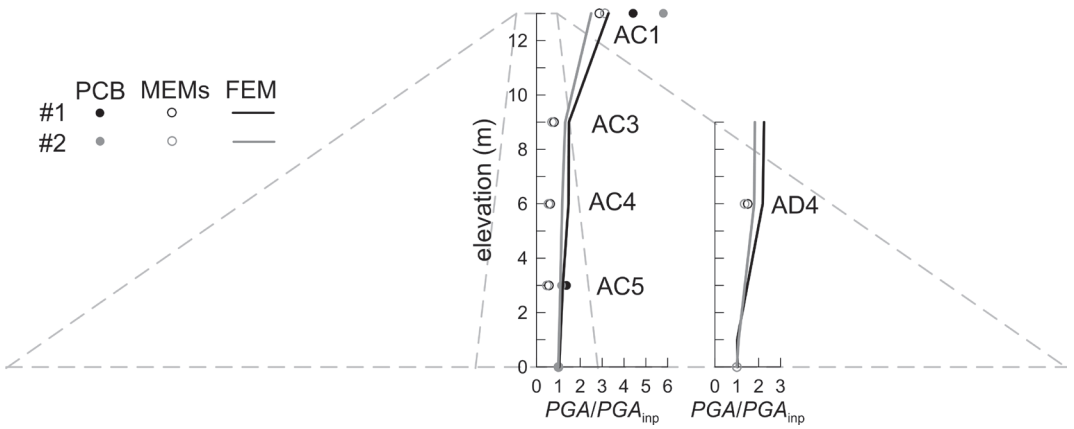

Fig. 16 – Profiles of the maximum accelerations in the core and in the downstream flank, normalised to the maximum acceleration of the input.

Fig. 16 – Profili dell'accelerazione massima nel nucleo e nel fianco di valle, normalizzati rispetto all'accelerazione massima applicata alla base della diga.

of the pore pressure and the value at the beginning of the first ground motion, disregarding the portion of the excess pore pressure still remaining in the core at the end of the impoundment phase.

Low excess pore pressures developed in both the fine core and the sandy flanks. As detailed by CASABLANCA *et al.* [2024], this could be attributed to two reasons. Firstly, the slope has been compacted to a state where the tendency to develop seismic positive excess pore pressures is limited. In addition, it is likely that the part of the embankment reached by the wet front was not fully saturated at the end of the impoundment phase. Therefore, the tendency to develop positive excess pore pressure is further reduced.

Although the F.E. simulations overpredict the maximum Δu due to the simplified assumption of the *HSsmall* model on the cyclic contractive/dilative response, the results of the analyses qualitatively agree with the observed behaviour. Moreover, the maximum values have little significance because they are attained instantaneously.

The Δu in the coarse-grained shells dissipated almost immediately after each ground motion, although the F.E. model predicts a somewhat slower response. The transducers located in the fine-grained core measured Δu values of less than 1 kPa, consistent with the small movements experienced by the core during ground motion (as detailed below). While close agreement between the measured and calculated response is observed at the intermediate height (TC5, Fig. 17e), the calculated Δu at the location of PC6 (Fig. 17d) appears to be overestimated when compared to the measured Δu. In particular, the F.E. model predicts an excess pore pressure Δu = 12 kPa during the strong motion phase of the first seismic input, which is not confirmed by the data from PC6. This aspect requires further investigation.

Figure 18 and figure 19 show the recorded and computed time histories of the vertical and horizontal displacements, while table VII summarises the final permanent displacements obtained as a result of the applied seismic sequence. The largest displacement gradients occur during the strong motion phase of the seismic input and are systematically larger for the second earthquake, which is characterised by approximately three times the Arias intensity of the first accelerogram. Figure 18 and figure 19 suggest a reasonable agreement between the numerical prediction and the observed behaviour, although the values calculated at the location of VU2 are significantly larger than those measured in the centrifuge.

The contours of the final vertical displacements computed at the end of Input #2 (Fig. 20) show that the largest values are localised in the upper part of the upstream flank (about -31.6 cm, 2.4%H at VU2), while the final permanent settlement of the core is negligible (-1 cm, 0.08%H at VC1, Tab. VIII). Therefore, the deformation pattern induced by the seismic sequence is characterised by downward sliding of the upstream slope, while the core remains mainly stable. Although the main mechanism is on the upstream side, the numerical analyses also provide non-negligible displacements on the downstream slope.

The same response can be observed by examining the contours of the final horizontal displacements (Fig. 21). Again, the largest values were calculated in the upstream slope (-26.9 cm, about 2%H at HU3). The permanent horizontal displacements of the core are negligible, while the maximum value in the downstream slope is about 7cm (0.5%H approximately at the location of VD3). The displacement field on the upstream side is deeper than that on the downstream side and is consistent with the trace of the pseudostatic critical sliding surface (dashed line in Fig. 21). The latter was obtained from an incremental pseudostatic analysis by applying, after the impoundment phase, a uniform horizontal body force expressed as a frac-

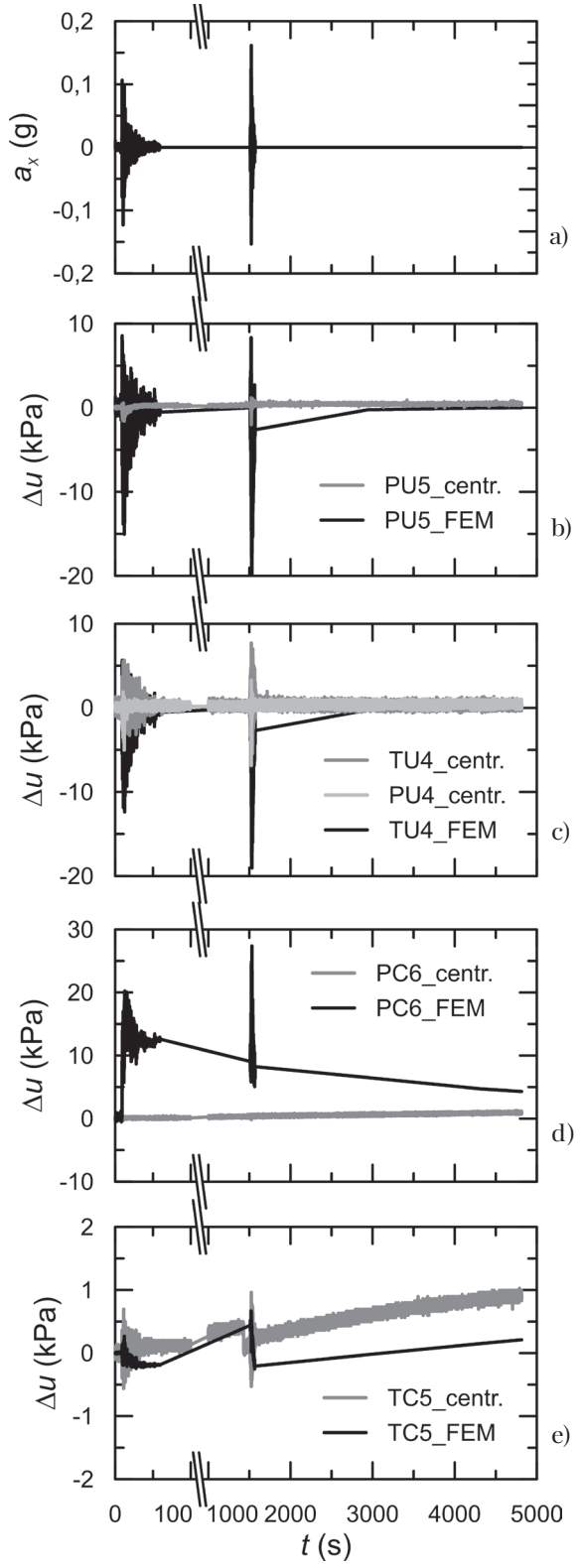

Fig. 17 – Time histories of the acceleration at the base of the model (a) and excess pore water pressure during the dynamic phases in the upstream flank (b, c) and the core (d, e): experimental vs numerical results.

Fig. 17 – Storie temporali dell'accelerazione alla base del modello (a) e della sovrappressione interstiziale durante le fasi dinamiche nel fianco di monte (b, c) e nel nucleo (d, e): confronto tra valori osservati e valori calcolati.

Tab. VII – Displacements (values in cm) at the end of the seismic phases: experimental vs numerical results.

Tab. VII – Spostamenti permanenti finali: confronto tra valori osservati e valori calcolati (in cm).

Transducer	centrifuge	FEM	centr./FEM (-)
VC1 (ver.)	-0.664	-1.054	0.630
VU2 (ver.)	-4.948	-31.58	0.157
VU3 (ver.)	-7.659	-13.22	0.579
HU3 (hor.)	-43.94	-25.84	1.700
VU4 (ver.)	-13.58	-10.17	1.335
VU5 (ver.)	-0.566	-5.561	0.102
HU5 (hor.)	-3.137	-17.71	0.177
VD4 (ver.)	-0.681	-2.631	0.259

tion k_h of gravity, the vertical component being constant and equal to gravity. The seismic coefficient k_h was gradually increased until convergence of the calculation algorithm was no longer possible. In particular, the sliding surface shown in figure 21 is associated with the minimum critical seismic coefficient $k_h = k_c = 0.075$. The deformation pattern obtained from the F.E. analyses is in good agreement with that observed at the end of the centrifuge tests, although the ratio between the calculated and measured displacements is in a wide range, between 0.157 and 1.700.

The stiff behaviour of the core can be ascribed to the effective suctions developed in the PON before the seismic loading. While the TS reaches the residual saturation for very low suction values (Fig. 9a), the PON is able to sustain sensibly higher suctions without attaining the residual condition. Therefore, the beneficial effect of the partial saturation is significant only in the fine-grained core, where $S_r^{eff} \neq 0$. In the downstream shell and in the partially saturated portion of the upstream slope $S_r^{eff} = 0$. As a result, the effective stress state and hence the available shear strength in the core is significantly higher than that in the shells. This aspect plays an important role in the seismic performance of the dam and can be highlighted by examining the stress state within the embankment using the relative shear stress $\tau_{rel} = \tau_{mob}/\tau_{max}$, where τ_{mob} is the radius of the current Mohr's circle and τ_{max} is the maximum value of the shear stress for the case where the Mohr's circle is extended to touch the Coulomb failure envelope while keeping the centre of the Mohr's circle constant. It represents the degree of shear strength mobilisation and is $\tau_{rel} = 1$ when the available shear strength is reached. Figure 22 shows the contours of τ_{rel} after the impoundment phase (Fig. 22a) and after the first seismic input (Fig. 22b).

The initial values of τ_{rel} in the core are significantly lower than those in the shells, where values above 0.9 can be observed near the surface of both slopes and near the crest. After input #1, full shear resistance is

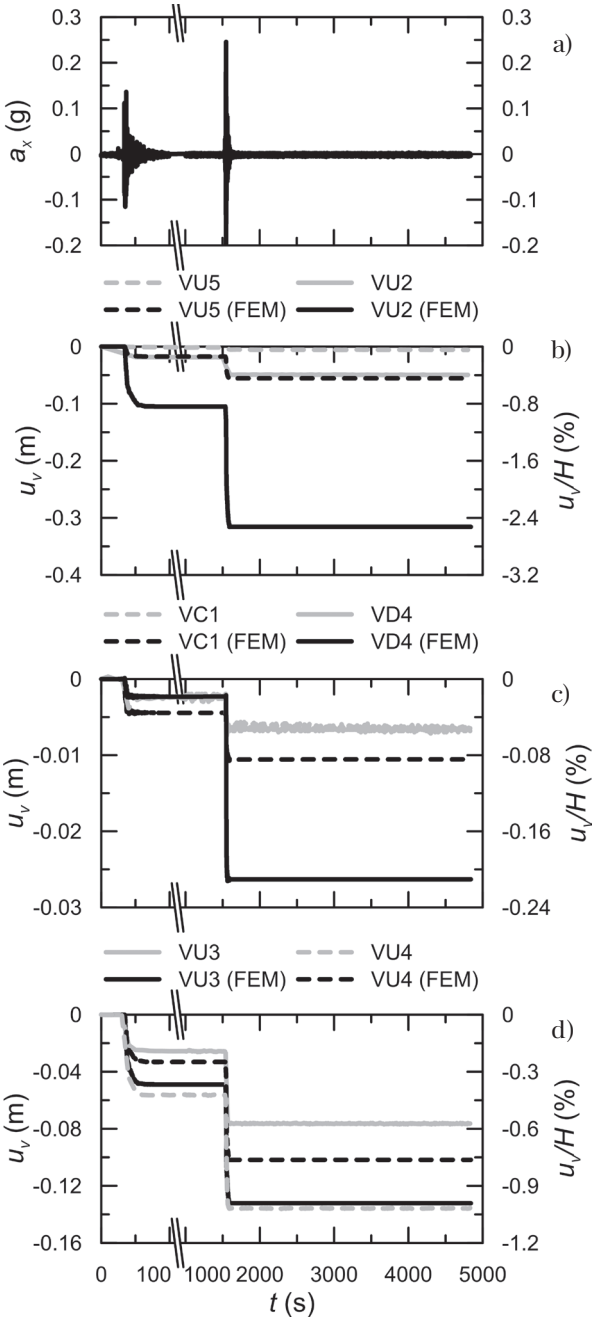

Fig. 18 – Time histories of the vertical displacements during the seismic phases: experimental vs numerical results.

Fig. 18 – Storie temporali degli spostamenti verticali misurati e calcolati durante la fase dinamica.

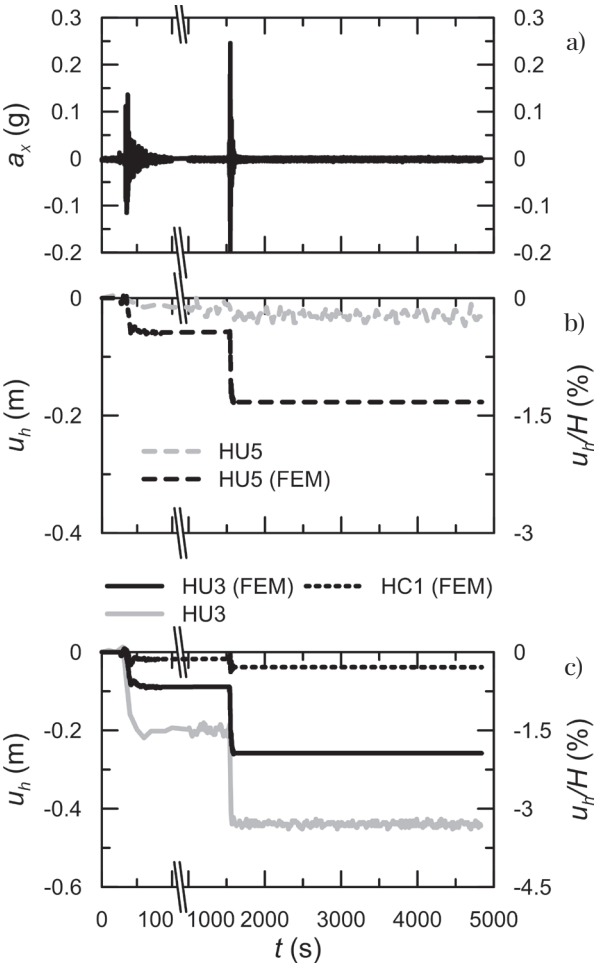

Fig. 19 – Time histories of the horizontal displacements during the seismic phases: experimental vs numerical results.

Fig. 19 – Storie temporali degli spostamenti orizzontali misurati e calcolati durante la fase dinamica.

almost reached in a large part of the upstream slope, with the development of deep shear bands similar to the pseudostatic sliding surface. The downstream flank also developed some shear bands where the available shear strength is fully mobilised, but they are shallower than those in the upstream slope. Therefore, the deformation pattern shown in figure 20 and figure 21 is the result of the transient mobilisation of the shear strength during the seismic shaking, with a progressive development of permanent displacements.

Finally, figure 23 shows the non-dimensional crest settlement u_v/H_{def} plotted against the input peak ground acceleration (*PGA*), where H_{def} indicates, for the case at hand, the dam height. In detail, the experimental and numerical results for the crest of the dam (transducer VC1) are shown, together with field observations collected by SWAISGOOD [2003] and the results obtained numerically by MASINI *et al.* [2021] and MASINI and RAMPELLO [2022] for a homogeneous and a zoned dam. Both the numerical and experimental results of this study are consistent with the reported literature data and indicate a negligible level of damage, confirming the satisfactory seismic performance of the dam.

4. Summary and conclusions

This paper has demonstrated the validity of the integrated experimental-numerical approach to the study of the seismic response of zoned earth dams.

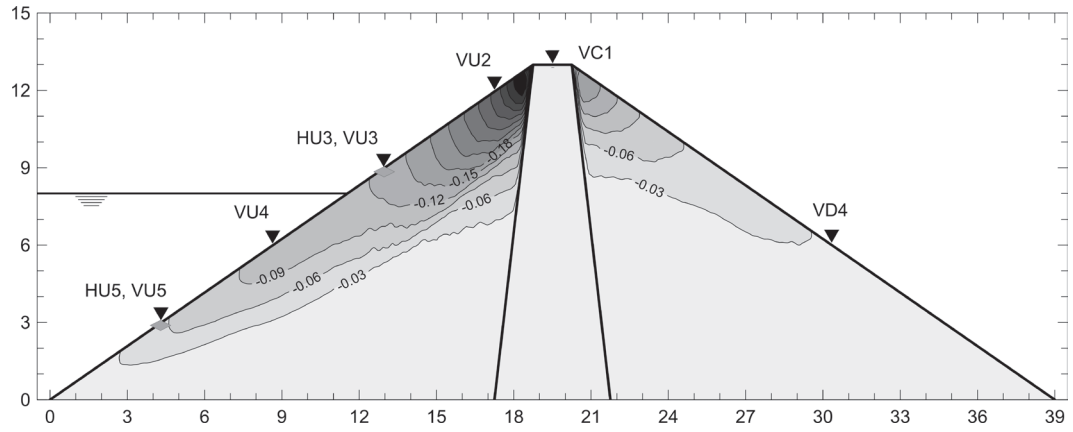

Fig. 20 – Contours of the vertical displacements at the end of the seismic events obtained from FE analyses (values in m).
Fig. 20 – Isolinee degli spostamenti verticali ottenuti dall'analisi numerica al termine dell'ultimo input sismico (valori in m).

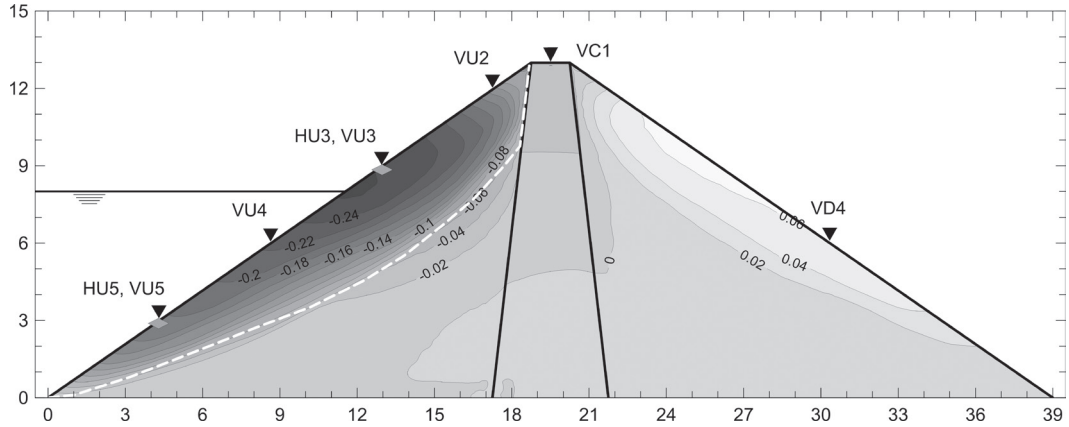

Fig. 21 – Contours of the horizontal displacements at the end of the seismic events obtained from FE analyses (values in m). White dashed line represents the trace of the slip surface obtained from numerical pseudostatic iterative analysis.
Fig. 21 – Isolinee degli spostamenti orizzontali ottenuti dall'analisi numerica al termine dell'ultimo input sismico (valori in m). La linea bianca tratteggiata rappresenta la traccia della superficie di scorrimento critica ottenuta da un'analisi pseudostatica iterativa.

Specifically, an FE model was initialised using monitoring data from the static phase of a centrifuge test on a zoned earth dam. The constitutive model adopted was carefully calibrated using the results of an extensive laboratory investigation carried out to characterise the mechanical and hydraulic properties of the test materials. The model simulated the main experimental procedure using a fully coupled hydromechanical (u-p) approach, explicitly considering the partial saturation state of the dam body. During the centrifuge test, data were collected on pore pressures, displacements and accelerations of the embankment. Two input motions, characterised by similar transient waveforms but different intensities, were applied to the base of the model. The predictive capacity of the model was assessed by comparing the computed and the observed behaviour. The main results of this study can be summarised as follows:

- The initialisation of the pore pressure values based on experimental data allows the hydraulic behaviour of the dam during the impoundment phase to be accurately simulated. In particular, the fully coupled flow-deformation approach allowed to obtain a close agreement between the numerical prediction and the observed behaviour in terms of the distribution and evolution of the pore pressure in the embankment.
- The numerical model was able to reproduce qualitatively the evolution of the excess pore pressure during the dynamic phases, although the values measured in the centrifuge test were systematically lower. This limitation of the model is attributed to the constitutive model adopted, which is not able to accurately reproduce the cyclic volumetric response of dense and partially saturated materials.
- Both the computed and observed response indicated that the impoundment of the reservoir caused negligible deformation of the earth dam.
- A significant amplification of the acceleration from the bottom to the base of the core was observed both experimentally and numerically, due to focalisation effects near the crest of the dam.

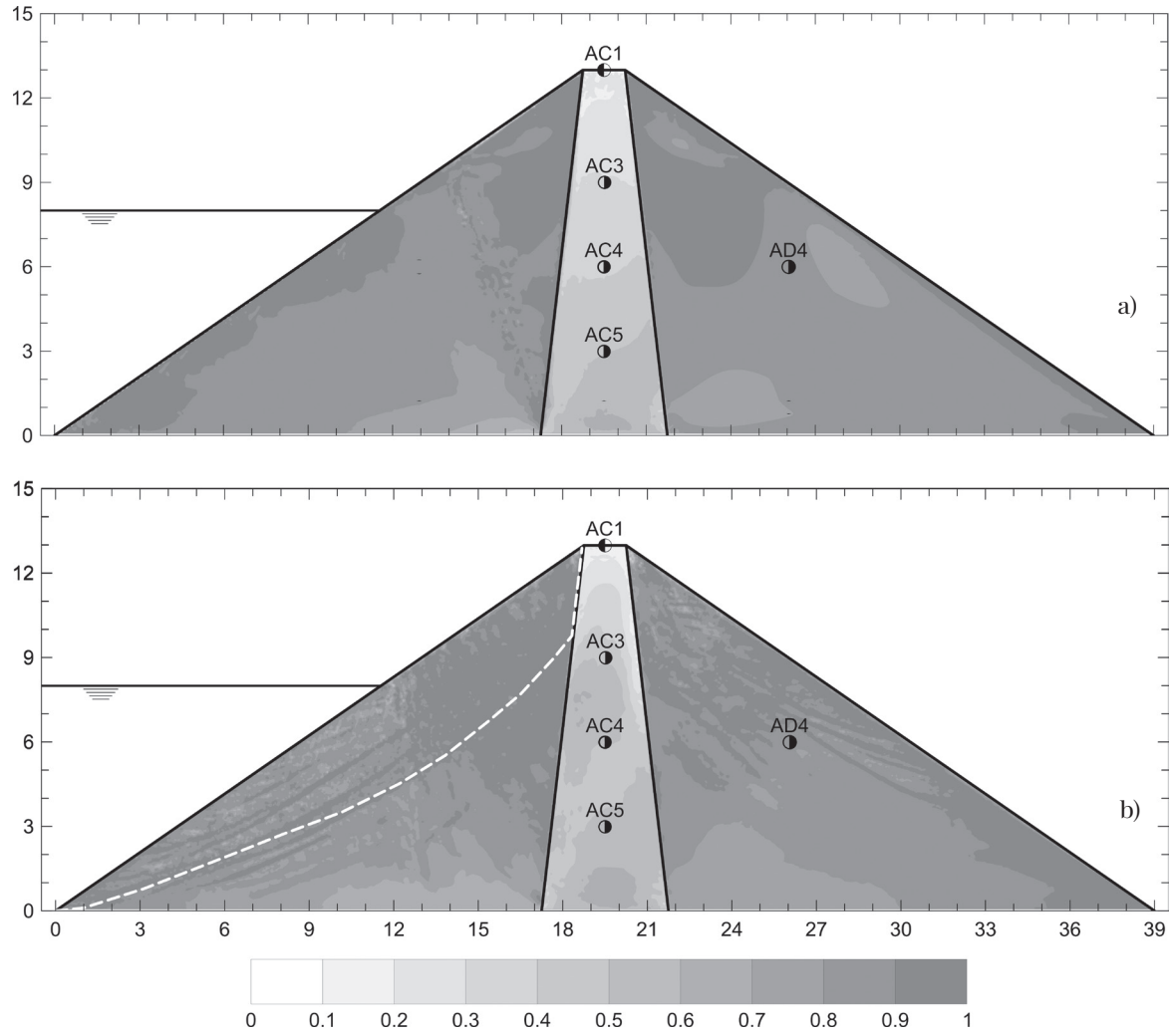

Fig. 22 – Contours of the relative shear stress τ_{rel} a) after the impoundment, and b) at the end of input #1.
Fig. 22 – Isolinee della tensione tangenziale relativa τ_{rel} a) al termine dell'invaso e b) alla fine dell'input #1.

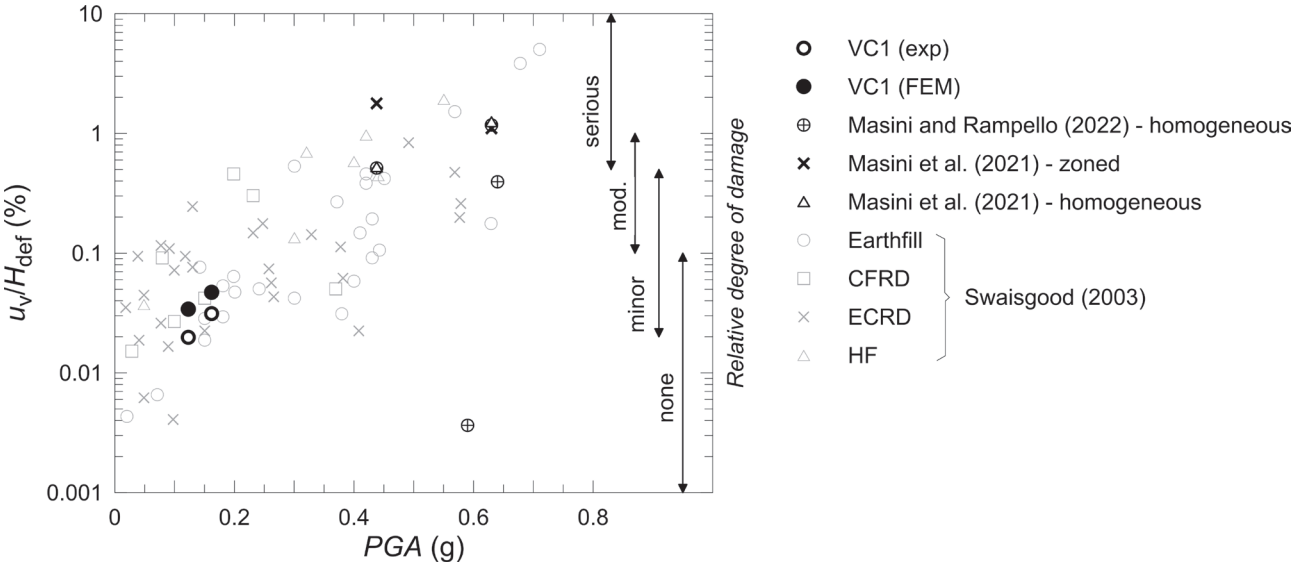

Fig. 23 – Non-dimensional crest settlement (u_v/H_{def}) as a function of the input peak ground acceleration (*PGA*).
Fig. 23 – Cedimento adimensionale della cresta della diga (u_v/H_{def}) in funzione della PGA.

The F.E. analyses provided maximum crest acceleration values in the range of 0.39 g to 0.49 g and profiles along the dam axis closer to those obtained from the data recorded by the MEMs. In contrast, the PCB accelerometers measured higher values, about twice as high as those derived from the numerical analyses. The fundamental frequency of the dam did not change as the intensity of the input motion increased, due to the stiff dynamic response of the core, which experienced small permanent displacements.

- The F.E. analyses confirmed the observed deformation pattern, which is characterised by a stiff response of the dam core due to pre-seismic effective suction in the fine-grained PON. This leads to an increased shear strength in the core compared to the shells. Consequently, the initial degree of shear mobilisation is lower in the core than in the shells, where the seismic shaking resulted in transient shear strength mobilisation and permanent displacements.
- The analyses also revealed the highly asymmetric response of the dam, with higher displacements affecting the upstream shell, as confirmed by the experimental observations.
- The mechanism identified on the upstream flank is also consistent with the result of a numerical pseudostatic iterative analysis. This provides a first estimation of an earth dam's seismic resistance through the critical seismic coefficient k_c, and has been shown to provide plastic mechanisms consistent with the displacement field observed in dynamic analyses. Therefore, the deformation pattern of an earth dam under strong ground motions is the consequence of a successive transient activation of plastic mechanisms that generate incremental permanent displacements. Although different ground motions result in different displacements, these are mainly driven by the same plastic mechanisms.
- The maximum measured and calculated seismic displacements were located at the top of the upstream flank, while the core was affected by negligible damage, confirming the satisfactory seismic performance of the dam for the seismic scenarios considered in this study.

Acknowledgements

The research work presented in this paper was funded by the research project PRIN 2017 REDREEF (Risk Assessment of Earth Dams and River Embankments to Earthquakes and Floods) supported by MIUR (Ministero dell'Istruzione, dell'Università e della Ricerca).

The centrifuge test was performed at the Istituto Sperimentale Modelli Geotecnici – ISMGEO (Bergamo, Italy) under the supervision of Prof. V. Fioravante and Prof. F. Giretti.

Finally, the authors would like to thank Dr. Ferdinando Marinelli for his support and fruitful discussions on the numerical analyses and Prof. Giovanni Biondi, Prof. Ernesto Cascone, Prof. Claudio Mancuso, Prof. Luca Pagano, Prof. Stefania Sica and Prof. Sebastiano Rampello for the precious supervision in the context of the research project.

References

Adalier K., Sharp M.K. (2004) – *Embankment dam on liquefiable foundation-dynamic behavior and densification remediation.* Journal of Geotechnical and Geoenvironmental Engineering, 130, n.11, pp. 1214-1224. doi.org/ 10.1061/(ASCE)1090-0241(2004)130:11(1214)

Aghamolaei M., Saeedi Azizkandi A., Ghalandarzadeh A. (2023) – *Evaluation of fault rupture propagation through earth dams subjected to reverse faulting: Outcomes from centrifuge simulation.* Soil Dynamics and Earthquake Engineering, 174, 108167. doi.org/ 10.1016/j.soildyn.2023.108167

Airoldi S., Fioravante V., Giretti D. (2018) – *Soil liquefaction tests in the ISMGEO geotechnical centrifuge.* Proceedings of China-Europe conference on geotechnical engineering, pp. 469-472.

Albano M., Modoni G., Croce P., Russo G. (2015) – *Assessment of the seismic performance of a bituminous faced rockfill dam.* Soil Dynamics and Earthquake Engineering, 75, pp. 183-198. doi.org/10.1016/j.soildyn.2015.04.005

Alonso E.E., Gens A., Josa A. (1990) – *A constitutive model for partially saturated soils.* Géotechnique, 40, n. 3, pp. 405-430.

Alonso E., Pinyol N. (2016) – *Numerical analysis of rapid drawdown: applications in real cases*. Water Science and Engineering, 9, n. 3, pp. 175-182. https://doi.org/10.1016/j.wse.2016.11.003

Andrianopoulos C.I., Papadimitriou A.G., Bouckovalas G.D., Karamitros D.K. (2014) – *Insight into the seismic response of earth dams with an emphasis on seismic coefficient estimation*. Computers and Geotechnics, 55, pp. 195-210. doi.org/10.1016/j.compgeo.2013.09.005

Argani L.P., Gajo A. (2022) – *A novel insight into vertical ground motion modelling in earthquake engineering.* Int J. Numer Anal Methods Geomech., 46, pp. 164-186. DOI: 10.1002/nag.3295

Arulanandan K., Scott R.F. (1993) – *Project VELACS Control Test Results*. Journal of Geotechnical Engineering, 119, n. 8. https://doi.org/10.1061/(ASCE)0733-9410(1993)119:8(1276)

Arulanandan K., Seed H.B., Yogachandran C., Muraleetharan K.K., Seed R.B. and Kabilamany K. (1993) – *Centrifuge study on volume changes and dynamic stability of earth dams*. Journal of Geotech-

nical Engineering, 119, n.11, pp.1717–1731. doi.org/ 10.1061/(ASCE)0733–9410(1993)119:11(1717)

BALDI G., BELLONI G., MAGGIONI W. (1988) – *The ISMES Geotechnical Centrifuge.* Proceedings of the international conference on geotechnical centrifuge modelling–Centrifuge 88, Paris, J. F. Corté (Ed.), Balkema, Rotterdam, pp. 45–48.

BELLOTTI R., JAMIOLKOWSKI M., PRESTI D.L., O'NEILL D.A. (1996) – *Anisotropy of small strain stiffness in Ticino sand.* Géotechnique, 46, n. 1, pp.115–131.

BENTLEY (2021) – *PLAXIS Connect Edition v21: A Finite Element Program for Geotechnical Engineering Problems.* Bentley Systems, Delft, The Netherlands.

BENZ T., VERMEER P.A., SCHWAB R. (2009) – *A small-strain overlay model.* Int. Journal for Numerical and Analytical Methods in Geomechanics, 33, pp. 25–44.

BILOTTA E., PAGANO L., SICA S. (2010) – *Effect of ground–motion asynchronism on the equivalent acceleration of earth dams.* Soil Dynamics and Earthquake Engineering, 30, n. 7, pp. 561–579. doi.org/ 10.1016/j.soildyn.2010.01.014

BIONDI G., CASCONE E., ALIBERTI D., RAMPELLO S. (2021) – *Screening-level analyses for the evaluation of the seismic performance of a zoned earth dam.* Engineering Geology, 280, 105954. doi.org/ 10.1016/j.enggeo.2020.105954

BISHOP A. W., BLIGHT G. E. (1963) – *Some aspects of effective stress in saturated and partly saturated soils*. Géotechnique, 13, n. 3, pp. 177–197.

BOULANGER R.W. (2019) – *Nonlinear Dynamic Analyses of Austrian Dam in the 1989 Loma Prieta Earthquake.* Journal of Geotechnical and Geoenvironmental Engineering, 145, n. 11, 05019011. doi.org/ 10.1061/(ASCE)GT.1943–5606.0002156

BUSCARNERA G., NOVA R. (2009) – *An elastoplastic strain hardening model for soil allowing for hydraulic bonding–debonding effects.* International journal for numerical and analytical methods in geomechanics, 33, n. 8, pp.1055–1086.

CASABLANCA O., NARDO A., BIONDI G., DI FILIPPO G., CASCONE E. (2022) – *Seismic performance of a zoned earth dam.* Proceeding of Conference on Performance-based Design in Earthquake – PBD 2022, Beijing, pp. 1929–1936.

CASABLANCA O., DI FILIPPO G., GIRETTI, D., MASINI L., ROLLO F., TRETOLA M., BIONDI G., CASCONE E., FIORAVANTE V., PAGANO L., RAMPELLO S., SICA S., MANCUSO C. (2024) – *Physical modelling of the dynamic response of a zoned earth dam*. Rivista Italiana di Geotecnica, 58, n. 4, pp. 9–29.

CASCONE E., BIONDI G., ALIBERTI D., RAMPELLO S. (2021) – *Effect of vertical input motion and excess pore pressures on the seismic performance of a zoned dam.* Soil Dynamics and Earthquake Engineering, 142:106566. doi.org/ 10.1016/j.soildyn.2020.106566

CHARATPANGOON B., KIYONO J., FURUKAWA A., HANSAPINYO C. (2014) – *Dynamic analysis of earth dam damaged by the 2011 Off the Pacific Coast of Tohoku Earthquake*. Soil Dynamics and Earthquake Engineering, 64, pp. 50–62. doi.org/10.1016/j.soildyn.2014.05.002

COSTIGLIOLA R.M., MANCUSO, C., PAGANO L., SILVESTRI F. (2022) – P*rediction of permanent settlements of an upstream faced earth dam.* Computers and Geotechnics, 144, 104594. doi.org/ 10.1016/j.compgeo.2021.104594

DI FILIPPO G., CASABLANCA O., BIONDI G., CASCONE E. (2023) – *Calibration of a large shaking table equipment for testing geotechnical physical models under plane strain conditions*. Soil Dynamics and Earthquake Engineering, 166, p. 107726.

ELIA G., AMOROSI A., CHAN A.H.C., KAVVADAS M.J. (2011) – *Fully coupled dynamic analysis of an earth dam*. Géotechnique, 61, n. 7, pp. 549–63.

ELIA G., ROUAINIA M. (2013) – *Seismic Performance of Earth Embankment Using Simple and Advanced Numerical Approaches.* Journal of Geotechnical and Geoenvironmental Engineering, 139, pp. 1115–1129. doi.org/10.1061/(ASCE)GT.1943–5606.0000840

FIORAVANTE V. (2000) – *Anisotropy of small strain stiffness of Ticino and Kenya sands from seismic wave propagation measured in triaxial testing*. Soils and foundations, 40, n. 4, pp.129–142.

FIORAVANTE V., JAMIOLKOWSKI M. (2005) – *Physical modelling of piled rafts. Proc. of the International Geotechnical Conference on Soil structure interaction: Calculation methods and Engineering Practice.* Saint Petersbourg–Moscow, pp. 89–95.

FIORAVANTE V., GIRETTI D. (2016) – *Unidirectional cyclic resistance of Ticino and Toyoura sands from centrifuge cone penetration tests.* Acta Geotechnica, 11, pp. 953–968.

FIORAVANTE V., GIRETTI D., AIROLDI S., MOGLIE J. (2021) – *Effects of seismic input, fine crust and existing structure on liquefaction from centrifuge model tests*. Bulletin of Earthquake Engineering, 19, pp. 3807–3833.

GALAVI V. (2010) – *Groundwater flow, fully coupled flow deformation and undrained analyses in PLAXIS 2D and 3D.* Plaxis internal report.

GE L., BAO Y., NI C.-K., KO H.-Y. (2010) – *Seismic centrifuge modelling of earth dams*. Geomechanics and Geoengineering, 5, n. 4, pp. 247–257. doi.org/ 10.1080/17486025.2010.492243

HAN B., ZDRAVKOVIC L., KONTOE S. (2016) – *Numerical and analytical investigation of compressional wave propagation in saturated soils.* Computers and Geotechnics, 75, pp. 93–102. doi.org/10.1016/j.compgeo.2016.01.019.

HARDIN B. O., DRNEVICH V. P. (1972) – *Shear modulus and damping in soils: design equations and curves.* Journal of the Soil mechanics and Foundations Division, 98, n. 7, pp.667–692.

IRSLAN KHALID M., PARK D., FEI J., NGUYEN V.-Q., NGUYEN D.-D., CHEN X. (2023) – *Selection of efficient earthquake intensity measures for evaluating seismic*

fragility of concrete face rockfill dam. Computers and Geotechnics, 163, 105721. doi.org/ 10.1016/j.compgeo.2023.105721

Izumi A., Sawada Y., Hori T., Maki R. (2021) – *Centrifuge modelling of small earth dams subjected to the combined effects of rainfall and earthquakes.* Soil Dynamics and Earthquake Engineering, 151, p. 106963. doi.org/ 10.1016/j.soildyn.2021.106963

Jaky J. (1944) – *The coefficient of earth pressure at rest*. Journal of the Society of Hungarian Architects and engineers, pp. 355–358.

Kim M.-K., Lee S.-H., Choo Y.W., Kim D.-S. (2011) – *Seismic behaviors of earthcore and concrete-faced rock-fill dams by dynamic centrifuge tests.* Soil Dyn. Earthquake Eng., 31, n. 11, pp. 1579–1593. https://doi.org/10.1016/j.soildyn.2011.06.010.

Kumar P., Viswanadham B.V.S. (2023) – *Centrifuge model studies on the performance of earthen dams with geocomposite internal drain subjected to pseudostatic seismic loading.* Soil Dynamics and Earthquake Engineering, 170,107907. doi.org/ 10.1016/j.soildyn.2023.107907

Kutter B.L. (1995) – *Recent Advances in Centrifuge Modeling of Seismic* Shaking. Proc. of 3rd international conference on recent advances in geotechnical earthquake engineering and soil dynamics, April 2–7, 1995, Volume II, St. Louis, Missouri, pp. 927–941, R. E. Taylor (Ed.) (2018) – Geotechnical centrifuge technology. CRC Press.

Lambe T. W. (1973) – *Predictions in soil engineering.* Géotechnique, 23, n. 2, pp. 151–202.

Mancuso C., Vassallo R., Vinale F. (2003) – *The behaviour of two unsaturated compacted soils used as construction materials.* In: Proc. of XIII Euro-pean Conference on Soil Mechanics and Foundation Engineering, Prague, Czech Republic, 2003, pp. 1–6.

Masini L., Rampello S., Callisto L. (2016) – *Seismic behaviour of large earth dams: from site investigations to numerical modelling.* Proceedings of the 1st IMEKO TC-4 Int. Workshop on Metrology for Geotechnics, Benevento, Italy, pp. 288–294.

Masini L., Rampello S., Donatelli R. (2019) – *Some aspects of the dynamic performance of two classes of earth dams.* Proceedings of the 7th International Conference on Earthquake Geotechnical Engineering – ICEGE 2019, Rome, Italy, pp. 3788–37957.

Masini L., Rampello S., Donatelli R. (2021) – *Seismic performance of two classes of earth dams*. Earthquake Engineering and Structural Dynamics, 50, n. 2, pp. 692–711. doi.org/ 10.1002/eqe.3352

Masini L., Rampello S. (2022) – *Influence of input assumptions on the evaluation of the seismic performance of earth dams.* Journal of Earthquake Engineering, 26, n. 9, pp. 4471–4495. doi.org/10.1080/13632469.2020.1835747

Ng C.W.W., Crous P.A., Jacobs S.W. (2023) – *Centrifuge and numerical modeling of liquefied flow and non-liquefied slide failures of tailings dams*. Journal of Geotechnical and Geoenvironmental Engineering, 149, n. 9, 04023075. doi.org/10.1061/JGGEFK.GTENG-10800

Papadimitriou A.G., Bouckovalas G.D., Andrianopoulos K.I. (2014) – *Methodology for estimating seismic coefficients for performance-based design of earthdams and tall embankments*. Soil Dynamics and Earthquake Engineering, 56, pp. 57–73. doi.org/10.1016/j.soildyn.2013.10.006

Park D.S., Kim N.-R. (2017) – *Safety evaluation of cored rockfill dams under high seismicity using dynamic centrifuge modeling.* Soil Dynamics and Earthquake Engineering, 97, pp. 345–363. doi.org/ 10.1016/j.soildyn.2017.03.020

Pelecanos L., Kontoe S., Zdravkovic L. (2015) – *A case study on the seismic performance of earth dams*. Géotechnique, 65, n. 11, pp. 923–935.

Pelecanos L., Kontoe S., Zdravković L. (2020) – *The Effects of Dam–Reservoir Interaction on the Nonlinear Seismic Response of Earth Dams*. Journal of Earthquake Engineering 24, n. 6, pp.1034–1056. doi.org/ 10.1080/13632469.2018.1453409

Rampello S., Cascone E., Grosso N. (2009) – *Evaluation of the seismic response of a homogeneous earth dam*. Soil Dynamics and Earthquake Engineering, 29, n. 5, pp. 782–798.

Rotisciani G. M., Desideri A., Amorosi A. (2021) – *Unsaturated structured soils: constitutive modelling and stability analyses.* Acta Geotechnica, 16, n. 11,pp. 3355–3380.

Saleh S., Madabhushi S. (2010) – *An investigation into the seismic behaviour of dams using dynamic centrifuge modelling.* Bull. Earthquake Eng., 8, n. 6, pp. 1479–1495. https://doi.org/10.1007/s10518-010-9183-9

Saleh S., Madabhushi S. (2011) – *Response of concrete dams on rigid and soil foundations under earthquake loading. J.* Earthquake Tsunami, 4, n. 3, pp. 251–268. https://doi.org/10.1142/S1793431110000820

Schanz T., Vermeer P.A., Bonnie P.G. (1999) – *Hysteretic damping in a small-strain stiffness model.* Proc. of the 10th Int. Symp. on Numerical Models in Geomechanics, NUMOG 10, London, pp. 737–742.

Sharp M.K., Adalier K. (2006) – *Seismic response of earth dam with varying depth of liquefiable foundation layer.* Soil Dynamics and Earthquake Engineering, 26, n. 11, pp. 1028–1037. doi.org/ 10.1016/j.soildyn.2006.02.007

Sica S., Pagano L., Modaressi A. (2008) – *Influence of past loading history on the seismic response of earth dams.* Comput. Geotech, 35, n. 1, pp. 61–85.

Sica S., Pagano L. (2009) – *Performance-based analysis of earth dams: procedures and application to a sample case.* Soils and Foundations, 49, pp. 912–925, ISSN: 0038-0806. doi: 10.3208/sandf.49.921

Sica S., Pagano L., Rotili F. (2019) – *Rapid drawdown on earth dam stability after a strong earthquake.* Comput. Geotech, 116, ISSN: 0266-352X. doi: 10.1016/j.compgeo.2019.103187

SICA S., DELLO RUSSO A. (2021) – *Seismic response of large earth dams in near-source areas.* Comput. Geotech, 132, ISSN: 0266-352X. doi: 10.1016/j.compgeo.2020.103807

SWAISGOOD J.R. (2003) – *Embankment dam deformations caused by earthquakes*. In: Proc. of the 2003 Pacific Conf. on Earthquake Eng., Christchurch NZ, 2003.

TAYLOR R.E. (Ed.) (2018) – *Geotechnical centrifuge technology.* CRC Press. London. doi. org/10.1201/9781482269321

TIAN C., LI Y., ZHANG X., ZHANG Z., HU J., SONG J., ZHANG X. (2023) – *Dynamic Centrifuge Experimental Study on Dam–Reservoir Interaction in Concrete-Face Rockfill Dams under Earthquake Loading.* International Journal of Geomechanics, 23, n. 12, p. 04023224. https://doi.org/10.1061/IJGNAI.GMENG-7857

VAN GENUCHTEN M. T. (1980) – *A closed-form equation for predicting the hydraulic conductivity of unsaturated soils.* Soil Science Society of America Journal, 44, n. 5, pp. 892-898.

VENTINI R., DODARO E., GRAGNANO C.G., GIRETTI D., PIRONE M. (2021) – *Experimental and numerical investigations of a river embankment model under transient seepage conditions.* Geosciences, 11, n. 5, p. 192.

VENTINI R., PIRONE M., MANCUSO C. (2023) – *Soil water retention curves of a silty clayey sand compacted at different dry density.* In: E3S Web of Conferences (382, p. 09007), EDP Sciences.

VENTINI R., MANCUSO C. (2024) – *Hydro-mechanical behaviour of Pontida sandy clayey silt compacted using two different pore fluids.* Rivista Italiana di Geotecnica, 58, n. 4, pp. 30-40.

VINALE F., D'ONOFRIO A., MANCUSO C., SANTUCCI DE MAGISTRIS F., TATSUOKA F. (1999) – *The pre-failure behaviour of soils as construction materials.* In: Proc. of II International Symposium on Pre-failure Deformation Characteristics of Geo-materials, Turin, Italy, 1999, pp. 955-1007.

WANG M., CHEN J., XIAO W. (2018) – *Experimental and numerical comparative study on gravity dam–reservoir coupling system.* Korean Society of Civil Engineers J. Civ. Eng., 22, pp. 3980-3987. https://doi.org/10.1007/s12205-018-1434-3

WU Q., LI D.-Q., LIU Y., DU W. (2021) – *Seismic performance of earth dams founded on liquefiable soil layer subjected to near-fault pulse-like ground motions*. Soil Dynamics and Earthquake Engineering, 143, p.106623. doi.org/ 10.1016/j.soildyn.2021.106623

YAMASHITA S., JAMIOLKOWSKI M., LO PRESTI D. C. L. (2000) – *Stiffness nonlinearity of three sands.* Journal of Geotechnical and Geoenvironmental Engineering, 126, n. 10, pp. 929-938

ZHANG, X., ZHANG, Z., WEI, Y., LIANG, J., HU J. (2019) – *Examining the seismic stress evolution in the face slab of concrete-faced rock-fill dams using dynamic centrifuge tests*. Soil Dynamics and Earthquake Engineering 123:337-356. https://doi.org/10.1016/j.soildyn.2019.05.008

ZHOU C., NG C. W. W., CHEN R. (2015) – *A bounding surface plasticity model for unsaturated soil at small strains*. International Journal for Numerical and Analytical Methods in Geomechanics, 39, n. 11, pp. 1141-1164.

ZIENKIEWICZ O. C., CHANG C. T., BETTESS P. (1980) – *Drained, undrained, consolidating and dynamic behaviour assumptions in soils.* Géotechnique, 30, n. 4, pp. 385-395.

ZIENKIEWICZ O. C., SHIOMI T. (1984) – *Dynamic behaviour of saturated porous media; the generalized Biot formulation and its numerical solution.* International journal for numerical and analytical methods in geomechanics, 8, n. 1, pp. 71-96.

Un approccio sperimentale/numerico per lo studio della prestazione sismica di una diga in terra zonata

Sommario

Le analisi numeriche dinamiche completamente accoppiate nel dominio del tempo rappresentano uno strumento efficace per la valutazione della prestazione sismica di dighe in terra, poiché consentono di tenere efficacemente in conto importanti aspetti quali la parziale saturazione, la complessa risposta dinamica del terreno e condizioni al contorno tipicamente non riproducibili mediante approcci di analisi più semplici. Tuttavia, la capacità previsionale di questi strumenti numerici dipende fortemente dalla corretta calibrazione e inizializzazione dei legami costitutivi adottati nelle analisi. A tal fine, è possibile ricorrere al confronto tra le simulazioni numeriche e il comportamento osservato dai dati di monitoraggio di casi di studio reali, oppure di modelli in scala ridotta testati nella centrifuga geotecnica.

Il presente lavoro descrive un approccio numerico/sperimentale integrato per studiare la prestazione sismica di una diga in terra zonata, in cui è stata modellata la risposta idromeccanica accoppiata in condizioni statiche e dinamiche del terreno. Il modello numerico è stato calibrato utilizzando i risultati di una prova in centrifuga geotecnica su una piccola diga in terra, simulando il processo di invaso e applicando un'azione sismica di intensità crescente. Il confronto tra le previsioni numeriche e i risultati della prova in centrifuga ha dimostrato la capacità del modello agli elementi finiti di riprodurre gli aspetti fondamentali del comportamento osservato. Inoltre è stato mostrato che l'approccio sperimentale e numerico integrato consente di sviluppare uno strumento di previsione robusto e affidabile che permette di studiare la risposta di sistemi geotecnici complessi come le dighe in terra durante eventi sismici molto intensi, di cui si hanno poche e lacunose osservazioni di casi reali. Infine sono state evidenziate alcune peculiarità nel comportamento di questa classe di strutture in terra, fornendo indicazioni per una valutazione razionale della loro prestazione sismica.